9. References

1. U.S. Nuclear Regulatory Commission, "Circumferential Cracking of Reactor Pressure Vessel Head Penetration Nozzles," NRC Bulletin 2001-01, August 3, 2001.

2. U.S. Nuclear Regulatory Commission, "Reactor Pressure Vessel Head Degradation and Reactor Coolant Pressure Boundary Integrity," NRC Bulletin 2002-01, March 18, 2002.

3. U.S. Nuclear Regulatory Commission, "Reactor Pressure Vessel Head and Vessel Head Penetration Nozzle Inspection Programs," NRC Bulletin 2002-02, August 9, 2002.

4. U.S. Nuclear Regulatory Commission, "Issuance of Order Establishing Interim Inspection Requirements for Reactor Pressure Vessel Heads at Pressurized Water Reactors," EA-03-009, February 11, 2003.

5. U.S. Nuclear Regulatory Commission, *An Approach for Using Probabilistic Risk Assessment in Risk-Informed Decisions on Plant–Specific Changes to the Licensing Basis*, Regulatory Guide 1.174, Revision 1, November 2002.

6. DEI Report R-3510-00-1, Revision 0, *Reactor Vessel Bolting Evaluations – HB Robinson 2 Nuclear Power Plant*, Dominion Engineering, Inc.

7. Letter from R. Barrett (NRC) to A. Marion (NEI) dated April 11, 2003, "Flaw Evaluation Guidelines." This document included two enclosures: Enclosure 1: *Flaw Evaluation Guidelines and Acceptance Criteria for PWR Reactor Vessel Upper Head Penetration Nozzles*, and Enclosure 2: *Appendix A: Evaluation of Flaws in PWR Reactor Vessel Upper Head Penetration Nozzles.*

8. P. C. Riccardella, "Probabilistic Fracture Mechanics Analysis of CRDM Nozzles," Presented at the NRC-MRP Meeting in Rockville, MD, June 12, 2003. NRC ADAMS Accession No. ML031740370.

9. *PWR Reactor Pressure Vessel (RPV) Upper Head Penetrations Inspection Plan (MRP-75): Revision 1*, EPRI, Palo Alto, CA: 2002. 1007337.

10. Attachment III to "Submittal of Information Requested by NRC Bulletin 2001-01, Circumferential Cracking of Reactor Pressure Vessel Head Penetration Nozzles," Docket No 50-261/ License No. DPR-23, Serial No. RNP-RA/01-0133, Progress Energy, September 4, 2001.

11. Letter from C. King (EPRI) to A. Marion and K. Cozens (NEI), MRP 2002-112, dated December 19, 2002.

12. W. H. Bamford, C. L. Hoffmann, and R. K. Perdue, *Development of a Technical Basis to Set the Inspection Interval for H. B. Robinson Reactor Vessel Head Penetrations*, Westinghouse Report WCAP-16110-P, July 2003.

13. *PWR Materials Reliability Program Response to NRC Bulletin 2001-01 (MRP-48)*, EPRI, Palo Alto, CA: 2001. 1006284.

14. IC-3515-00-2, "Record of Lead Review of Draft of R-3515-00-1," from Ted Huminski (H. B. Robinson) to G. A. White (DEI), EGR-NGGC-0003, dated June 18, 2003, Item No. 8.

15. "Submittal of Information Requested by NRC Bulletin 2001-01, Circumferential Cracking of Reactor Pressure Vessel Head Penetration Nozzles," Docket No 50-261/ License No. DPR-23, Serial No. RNP-RA/01-0133, Progress Energy, September 4, 2001.

16. "Submittal of Information Requested by NRC Bulletin 2002-01, Reactor Pressure Vessel Head Degradation and Reactor Coolant Pressure Boundary Integrity," Serial No. RNP-RA/02-0041, Progress Energy, April 1, 2002.

17. *Visual Examination for Leakage of PWR Reactor Head Penetrations on Top of RPV Head: Revision 1 of 1006296, Includes Fall 2001 Inspection Results*, EPRI, Palo Alto, CA: 2002. 1006899.

18. "Submittal of Results of Reactor Pressure Vessel Head and Vessel Head Penetration, Nozzle Inspections Performed During Refueling Outage 21," Serial No. RNP-RA/02-0175, Progress Energy, December 13, 2002.

19. "Response to Request for Additional Information Regarding 60-Day Response to NRC Bulletin 2002-01, Reactor Pressure Vessel Head Degradation and Reactor Coolant Pressure Boundary Integrity," Serial No. RNP-RA/03-0001, Progress Energy, January 31, 2003.

20. Email from J. P. Lareau (Westinghouse) to W. H. Bamford (Westinghouse), "RPVH PODs," dated April 14, 2003.

21. A. P. Berens and P. W. Hovery, *Evaluation of NDE Reliability Characterization*, Air Force Wright Aeronautical Laboratories, AFWAL-TR-81-4160, Volume 1, December 1981.

22. "Eddy Current Examination Technique Data Sheet ETSS # 20511.1," Rev. 5, Feb. 2003, for 200 and 300kHz Plus Point examinations of axial PWSCC in tubes of thicknesses between 0.043 to 0.050 in., EPRIQ.com database.

23. T. R. Gurney, *Fatigue of Welded Structures*, Cambridge University Press, Second Edition, 1979, pp. 48-53.

24. T. Alley, "Status of Reactor Vessel Head Penetration Inspection Activities," Presented at the NRC-MRP Meeting in Rockville, MD, June 12, 2003. NRC ADAMS Accession No. ML0317401401.

25. Email from W. H. Bamford (Westinghouse) to G. A. White (DEI), "Flaw shape from actual flaws in Alloy 182 welds," dated July 10, 2003.

26. *PWSCC of Alloy 600 Materials in PWR Primary System Penetrations*, EPRI, Palo Alto, CA: 1994. TR-103696.

27. R. Abernethy, *The New Weibull Analysis Handbook, 4th Edition*, Published by the author, 536 Oyster Rd., North Palm Beach, FL 33408-4328, September 2001.

28. *Steam Generator Degradation Database Version 3.0: User Manual*, EPRI, Palo Alto, CA: 2002. 1006663.

29. *Statistical Analysis of Steam Generator Tube Degradation*, EPRI, Palo Alto, CA: 1991. NP-7493.

30. *Statistical Analysis of Steam Generator Tube Degradation: Additional Topics*, EPRI, Palo Alto, CA: 1994. TR-103566.

31. *PWSCC Prediction Guidelines*, EPRI, Palo Alto, CA: 1994. TR-104030.

32. *A Model of the Effects of Li, B, and H_2 on Primary Water Stress Corrosion Crack Initiation in Alloy 600 (MRP-68)*, EPRI, Palo Alto, CA: 2002. 1006888.

33. R. W. Staehle, "Bases for Predicting the Earliest Failures Due to Stress Corrosion Cracking," *Chemistry and Electrochemistry of Corrosion and Stress Corrosion Cracking: A Symposium Honoring the Contributions of R. W. Staehle*, The Minerals, Metals & Materials Society (TMS), Warrendale, PA: 2001. pp. K-1–K-92.

34. J. I. Bennetch, "Root Cause Evaluation and Repair of Alloy 82/182 J-groove Weld Cracking of Reactor Vessel Head Penetrations at North Anna Unit 2," ASME PVP-Vol. 437, PVP2002-1189, 2002, pp. 179-186.

35. *Materials Reliability Program (MRP) Crack Growth Rates for Evaluating Primary Water Stress Corrosion Cracking (PWSCC) of Thick-Wall Alloy 600 Materials (MRP-55) Revision 1*, EPRI, Palo Alto, CA: 2002. 1006695.

36. *Crack Growth of Alloy 182 Weld Metal in PWR Environments (PWRMRP-21)*, EPRI, Palo Alto, CA: 2000. 1000037.

37. S. Le Hong, J. M. Boursier, C. Amzallag, and J. Daret, "Measurements of Stress Corrosion Cracking Growth Rates in Weld Alloy 182 in Primary Water of PWR," *Tenth International Conference on Environmental Degradation of Materials in Nuclear Power*

Systems—Water Reactors (Lake Tahoe, Nevada, August 5-9, 2001), NACE International, The Corrosion Society, Volume 1, Paper 33.

38. R. Lindström, P. Lidar, and J. Lagerström, "Crack Growth of Alloy 182 in a Simulated Primary Side PWR Environment," *Eighth International Symposium on Environmental Degradation of Materials in Nuclear Power Systems—Water Reactors* (Amelia Island, FL, August 10-14, 1997), Edited by S. M. Bruemmer, American Nuclear Society (ANS), La Grange Park, IL, 1997, pp. 422–429.

39. C. M. Brown and W. J. Mills, "Effect of Water on Mechanical Properties and Stress Corrosion Behavior of Alloy 600, Alloy 690, EN82H Welds, and EN52 Welds," *Corrosion*, Vol. 55, No. 2, 1999, pp. 173.

40. B. Wilson, "Inspection and Repair Strategy for Reactor Vessel Head Penetrations in Ringhals," *Proceedings: 1992 EPRI Workshop on PWSCC of Alloy 600 in PWRs*, EPRI, Palo Alto, CA: 1993. TR-103345, Paper B3.

41. H. Sjöstrand, "Ringhals Unit #2, #3 and #4 RVHP Examination Results from NDE and Boat Sample Analysis," *Proceedings: 1994 EPRI Workshop on PWSCC of Alloy 600 in PWRs*, EPRI, Palo Alto, CA: 1995. TR-105406, Part 1, Paper A3.

42. "Oconee Unit 1, 2, and 3 Vessel Head Penetration Inspection, Results and Metallurgical Laboratory Results." Duke Power, pp. 16-20. *Information-only document provided to DEI by Duke Power.*

43. "Oconee Unit 1, 2, and 3 Vessel Head Penetration Inspection, Results and Metallurgical Laboratory Results." Duke Power, p. 33. *Information-only document provided to DEI by Duke Power.*

44. "Reactor Vessel Head and Penetration Nozzle Condition Report," Letter from Duke Energy to NRC, Docket No. 50-270, Oconee Nuclear Station Unit 2, dated December 23, 2002, pages 2, 3, and 11 of attachment.

45. I. S. Raju and J. C. Newman, "Stress Intensity Factor Influence Coefficients for Internal and External Surface Cracks in Cylindrical Vessels," *Aspects of Fracture Mechanics in Pressure Vessels and Piping*, ASME PVP Vol. 58, 1982, pp. 37-48.

46. A. Zahoor, "Section 1.5, Internal Flaw, Arbitrary Stress Distribution, $1 \leq R_i/t \leq 10$," in Chapter 8, "Finite Length, Axial Part-Throughwall Flaw," in Volume 3 of *Ductile Fracture Handbook*, EPRI, Palo Alto, CA: 1989. NP-6301-D.

47. W. H. Bamford and C. Y. Yang, *Structural Integrity Evaluation of Reactor Vessel Upper Head Penetrations to Support Continued Operation: H. B. Robinson Unit 2*, Westinghouse Report WCAP-15928, August 2002.

48. W. J. Shack, "Parametric Studies of the Probability of Failure of CRDM Nozzles," Argonne National Laboratory, Presented at the NRC Nuclear Safety Research Conference, Washington, DC, NUREG/CP-0180, October 28-30, 2002.

49. ASME Boiler and Pressure Vessel Code, Section XI, Paragraph IWB-3640 and Paragraph IWB-3644, July 1, 2002 addenda.

50. Combustion Engineering Drawings for Westinghouse Electric Corporation 155.5" ID Reactor Vessel:

    a. Combustion Engineering Drawing No. E-232-271, Revision 4, General Arrangement – Elevation.

    b. Combustion Engineering Drawing No. E-232-279, Revision 7, Closure Head Assembly.

    c. Combustion Engineering Drawing No. E-232-284, Revision 5, Control Rod Mechanism Housing Details.

    d. Combustion Engineering Drawing No. E-232-285, Revision 3, Control Rod Penetration Details.

51. *Ductile Fracture Handbook*, EPRI, Palo Alto, CA: 1989. NP-6301-D.

52. *PWR Material Reliability Program, Interim Alloy 600 Safety Assessments for US PWR Plants (MRP-44): Part 2: Reactor Vessel Top Head Penetrations,* EPRI, Palo Alto, CA: 2001. TP-1001491, Part 2.

53. DEI Report R-3513-00-1, Revision 1, *Reactor Vessel Top Head Nozzle - Operating Fit Analysis – H.B. Robinson 2 Nuclear Power Plant*, Dominion Engineering, Inc.

54. Email from B. Dolan (H. B. Robinson) to R. K. Perdue (Westinghouse), "Small LOCA Birnbaum measure," dated April 8, 2003.

55. IC-3515-00-3, Email from B. Dolan (H. B. Robinson) to G. A. White (DEI), "RNP head inspection deferral," dated July 3, 2003.

56. U.S. Nuclear Regulatory Commission, "Potential Impact of Debris Blockage on Emergency Sump Recirculation at Pressurized-Water Reactors," NRC Bulletin 2003-01, June 9, 2003.

57. IC-3515-00-1, Email from E. Caba (H. B. Robinson) to G. A. White (DEI), "Reference Approval," dated July 21, 2003.

58. E-mail from R. Y. Schonenberg (Dominion Power) to G. A. White (DEI), "Millstone 2 RPV Closure Head Nozzle Data," dated July 1, 2003. *Information-only document.*

59. IC-3515-00-4, Email from Ted Huminski (H. B. Robinson) to E. S. Hunt (DEI), dated April 15, 2003.

60. "Inconel Alloy 600," Special Metals Product Literature. *Information-only document.*

61. ASME Boiler and Pressure Vessel Code, Section XI, Appendix A-3000, July 1, 2002 addenda.

APPENDICES

Appendix A

Stress Analysis of Robinson CRDM Nozzles

Attached calculation note C-3515-00-1, Revision 0, *H.B. Robinson CRDM Nozzle Stress Analysis*, provides results of elastic-plastic finite element analyses of four Robinson CRDM nozzles at angles of 0.0°, 9.3°, 27.1°, and 46.0°. The analyses were performed using the highest yield strength of any of the Robinson nozzles. The results of this analysis are used as input to the crack tip stress intensity factor calculations in Appendix B.

Attached calculation note C-3515-00-3, Revision 0, *Stress Comparison of Nominal and As-Built CRDM Nozzle Geometries at H. B. Robinson*, provides analysis results for the same four nozzles as noted in the preceding paragraphs, but with the as-built weld profile determined by the NDE inspection. As discussed in Section 4, the NDE showed that the fillets between the nozzles and the J-groove welds on the downhill sides of the nozzles are larger than specified on the design drawings. This calculation note also compares the stresses for the two cases. The conclusion from this work is that the larger fillet results in the weld toe being at an elevation with lower restraint from the vessel head such that the stresses at the weld toe are lower than for the as-designed case. The deterministic and probabilistic analyses in Section 7 and 8 were performed using the more conservative results for the as-designed cases.

The contents of Appendix A are proprietary to DEI.

Confidential Commercial Information

[DEI Calculation C-3515-00-1, Revision 0, *H.B. Robinson CRDM Nozzle Stress Analysis*, is proprietary to Dominion Engineering, Inc., and has been removed from this non-proprietary version of Appendix A.]

Confidential Commercial Information

[DEI Calculation C-3515-00-3, Revision 0, *Stress Comparison of Nominal and As-Built CRDM Nozzle Geometries at H. B. Robinson*, is proprietary to Dominion Engineering, Inc., and has been removed from this non-proprietary version of Appendix A.]

Appendix B

Stress Intensity Factors and Crack Growth Time

The purpose of Appendix B is to calculate stress intensity factors and crack growth times for the Robinson CRDM penetrations for axial ID and OD nozzle flaws, radial weld flaws, and through-wall circumferential flaws located above the root of the J-groove weld. Appendix B concludes with an evaluation of the rate of crack growth for multiple circumferential cracks initiating on the nozzle OD surface above the root of the J-groove weld. This evaluation shows that the model for circumferential crack growth based on a through-wall flaw having an initial total arc size of 30° predicts nozzle ejection to occur sooner than would a model based on circumferential crack growth from multiple initiation sites on the nozzle OD.

B.1 Axial ID Flaw in Nozzle

The following inputs are used to evaluate axial ID flaw stress intensity factors and crack growth times:

- Welding residual and operating stresses from calculation C-3515-00-1, Rev. 0 (Appendix A),
- Nozzle OD = 4.000 inches,
- Nozzle ID = 2.750 inches,
- Flaw evaluation methodology specified in the current NRC guidance (7),
- Operating head temperature of 599.7°F per (14).

a. Stress Intensity Factor Calculation Method

The first step in calculating axial ID flaw stress intensity factors and crack growth times is to characterize the flaw depth (a), length (ℓ, or $2c$) and location, with respect to the top and bottom of the weld. Evaluation of the axial cracks differs depending on the elevation of the crack with respect to the weld, since the hoop stress (σ) changes with the elevation. The hoop stress is usually maximum in the weld region and decreases from the top of the weld to the top of the penetration.

The through-wall hoop stress distribution that drives axial crack growth is taken from DEI calculation C-3515-00-1 (Appendix A). As described in that calculation, four nozzle penetration geometries (at 0.0°, 9.3°, 27.1°, and 46.0°) are considered to cover the range of penetration angles at Robinson. As shown in Figure 8-3, bounding yield strength values were chosen for the four stress analysis cases. The stress calculation includes welding residual stresses, the effect of hydrostatic testing which provides some mechanical stress relief, and operating temperature and pressure. A review of the plots of hoop stress for the four models from C-3515-00-1 demonstrates that the

maximum hoop stresses occur at the uphill and downhill sides of the nozzle; therefore, only these two cases are considered. Finally, DEI calculation C-3515-00-3 (Appendix A) shows that the somewhat larger as-built downhill side weld profile in comparison to the design profile does not produce any significant increases in the magnitude of the hoop and axial stresses that are used in the stress intensity factor calculations described below for the various flaw geometries (axial ID, axial OD, surface weld, and circumferential OD). In fact, the stresses that drive axial crack growth upward on the nozzle OD on the downhill side below the weld toe are lower in the case of the estimated as-built weld profile.

The current NRC flaw evaluation guidance (7) specifies that the crack tip stress intensity factor (K) may be calculated using the method developed by Raju and Newman (45). Calculations were performed using the Raju-Newman method and another model from Zahoor (46).

Raju and Newman Model

The Raju-Newman model involves fitting a third order polynomial to the through-thickness hoop stress distribution of the form:

$$\sigma_{\theta\theta} = \sum_{j=0}^{3} A_j z^j \qquad \text{[Eq. B-1]}$$

where:

A_j	=	polynomial coefficient for j^{th} order term
z	=	distance from crack mouth
$\sigma_{\theta\theta}$	=	hoop stress

Then, the stress intensity factor can be calculated using the following equation:

$$K_I = \sqrt{\pi \frac{a}{Q}} \times \sum_{j=0}^{3} G_j(a/c, a/t, t/R, \phi) A_j a^j \qquad \text{[Eq. B-2]}$$

where:

Q	=	Shape factor for an elliptical crack, approximated in (45) as $Q = 1 + 1.464(a/c)^{1.65}$
a	=	Depth of surface crack
c	=	Half length of the surface crack
G_j	=	Influence coefficient for j^{th} stress distribution
K_I	=	Stress intensity factor

The G_j values for ID cracks in a cylinder with a t/R ratio of 0.1 and 0.25 are provided in Tables 1 and 2 of the Raju-Newman paper (45). Influence coefficients are provided for crack aspect ratios (a/c) of 0.2, 0.4, and 1.0 ($a/2c$ from 1/10 to 1/2).

Zahoor Model

The Zahoor model also involves fitting a third order polynomial to the through-thickness hoop stress distribution:

$$\sigma_i = \sigma_0 + \sigma_1(z/t) + \sigma_2(z/t)^2 + \sigma_3(z/t)^3 \qquad \text{[Eq. B-3]}$$

The σ_i are coefficients of the stress polynomial describing the hoop stress (σ) variation through the cylinder wall (z is the distance from the inner surface and t is the wall thickness).

The stress intensity factor can be calculated using the following equation:

$$K_I = (\pi t)^{0.5}[\sum_{i=0}^{3} \sigma_i G_i] \qquad \text{[Eq. B-4]}$$

where:

G_i = shape factors associated with the coefficients of the stress polynomial σ_i for an ID axial part-through wall flaw of finite length, expressed by:

$G_i = A_0 + (A_1\alpha_i + A_2\alpha_i^2 + A_3\alpha_i^3 + A_4\alpha_i^4 + A_5\alpha_i^5)/[0.102(R_i/t) - 0.02]^{0.05}$

$\alpha_i = (a/t)/(a/c)^m$

The values of A_0 through A_5 and m in the above relationship for G_i are given in Table 8.1-1 of Zahoor (46) for each G_i. R_i is the cylinder inner radius, a the flaw depth at deepest point, and c the flaw half length.

For both the Raju-Newman and Zahoor methods, the through-thickness stress distributions for ID axial flaws were evaluated at different elevations. To be conservative, the elevation that gives the highest crack growth rate has been retained in all cases, which was usually at the elevation of the root of the weld. Figure B-1 shows a typical location of the assumed flaw on the ID of the nozzle. Figures B1-1 through B1-4.b show the through-wall hoop stress distributions for the selected locations. (These figures do not include the point at the weld/tube interface (z = 0.625 inches) because stress averaging across two dissimilar materials is performed at that location as part of the standard finite-element analysis technique.)

Stress intensity calculations for both models include various parameters, such as the crack depth and the a/c ratio. The calculations start with a crack depth of 0.04 inches (1.0 mm) because this is the expected detectability limit for an ECT inspection (see paragraph 5.7), but the PFM model of Section 8 allows for selection of a variable initial depth for the probabilistic calculations. Various a/c ratios have been considered since the stress intensity factor coefficients increase as a/c decreases (ℓ/a increases). To be conservative, a low a/c ratio of 1/3 (ℓ/a = 6) has been retained for all calculations. This ratio is assumed to cover most of the crack aspect ratios found in service experience.

Figures B1-5 through B1-8.b show the stress intensity factors calculated for the stress distributions in Figures B1-1 through B1-4.b, respectively.

b. Crack Growth Rate Calculation Method

The crack growth rate in Alloy 600 nozzle material is computed using the method specified in the current NRC guidance (7), which lists the crack growth rate equation from MRP-55 (35). Specifically:

$$\dot{a} = \exp\left[-\frac{Q_g}{R}\left(\frac{1}{T}-\frac{1}{T_{ref}}\right)\right]\alpha\left(K-K_{th}\right)^{\beta} \qquad \text{[Eq. B-5]}$$

where:

$\dot{a}$	=	crack growth rate at temperature T (m/s, or in/yr)
Q_g	=	thermal activation energy for crack growth
	=	130 kJ/mole (31.0 kcal/mole)
R	=	universal gas constant
	=	8.314×10^{-3} kJ/mole·K (1.103×10^{-3} kcal/mole·°R)
T	=	absolute operating temperature at crack location (599.7°F)
	=	588.54 K (1059.37°R)
T_{ref}	=	absolute reference temperature used to normalize crack growth data (325°C) = 598.15 K (1076.67°R)
α	=	crack growth rate coefficient
	=	2.67×10^{-12} at 325°C for $\dot{a}$ in units of m/s and K in units of MPa$\sqrt{m}$
	=	3.69×10^{-3} at 617°F for $\dot{a}$ in units of in/yr and K in units of ksi$\sqrt{in}$
K	=	crack tip stress intensity factor, MPa$\sqrt{m}$ (or ksi$\sqrt{in}$)
K_{th}	=	apparent crack tip stress intensity factor threshold for SCC
	=	9 MPa$\sqrt{m}$ (8.19 ksi$\sqrt{in}$)
β	=	exponent = 1.16

The results of the crack growth calculations for ID axial flaws are shown in Figures B1-9 through B1-12.b. These figures show the relative flaw depth (a/t) as a function of time computed using the crack tip stress intensity factors in Figures B1-5 through B1-8.b and the crack growth equation defined above. The curves based on the Raju-Newman and Zahoor methods show good agreement in all cases. The Raju-Newman model results were selected as the input for the probabilistic calculations in Section 8, since this method is the one identified in the current NRC guidance (7), and are reflected in Table B-1.

Note that in all cases the minimum stress intensity factor input to the crack growth rate equation—in particular for the Raju-Newman model results—was greater than approximately 14.5 MPa$\sqrt{m}$. This matches the approximate lower bound of 15 MPa$\sqrt{m}$ cited in MRP-55 (35) for the laboratory data used to develop the above crack growth equation for thick-section Alloy 600 material. Moreover, the minimum stress intensity factors input to the crack growth rate equation for the other modeled

flaw geometries (OD axial, radial weld, and through-wall OD circumferential) were also greater than at least approximately 14.5 MPa$\sqrt{m}$.

B.2 Axial OD Flaw in Nozzle

The first step in calculating axial OD flaw stress intensity factors and crack growth times is to characterize the flaw depth (a), length (ℓ, or $2c$) and location, in particular the distance between the top edge of the flaw and the bottom of the weld. Evaluation of the axial cracks differs depending on the elevation of the crack with respect to the weld, since the hoop stress (σ) changes with the elevation. The hoop stress is usually maximum in the weld region and decreases from the bottom of the weld to the bottom of the nozzle.

a. Stress Intensity Factor Calculation Method

The current NRC flaw evaluation guidance (7) specifies that the crack tip stress intensity factor (K) may be calculated using the method developed by Raju and Newman (45), as described in paragraph B.1 for axial ID flaws. The G_j coefficients involved in the method are a function of a/c, a/t, t/R, and also ϕ, the angular location around the crack front. It is then possible to calculate the stress intensity factor on the upper edge of a surface flaw growing both in depth and in length toward the bottom of the weld and beyond. The OD flaw would then be modeled to grow to the top of the weld, creating a possible leak path. This is a more conservative case than an OD flaw growing first through-wall and then up to the top of the weld, and is consistent with the axial OD cracking that has been observed. Therefore, K at the upper edge of an axial OD flaw can be calculated using the coefficients from Tables 3 and 4 of Reference (45) for an angle of 0° from the free surface. The Zahoor model parameters are only available for stress intensity factor calculations at the maximum depth point, and have not been used in this section.

The stress intensity factors using the Raju-Newman method were calculated at different elevations for the eight geometries described above (four nozzle angles and the uphill and downhill sides). Then, as before, the through-wall hoop stress distribution was fit to a cubic polynomial. Figures B2-1 through B2-4.b show the through-wall hoop stress distributions at the elevation of the bottom (toe) of the weld.

The most conservative case would be for a flaw to initiate at the bottom of the weld, since the hoop stress increases from the bottom of the nozzle to the bottom of the weld, and it would also require less time for the crack to reach the top of the weld. This case has been selected for all the calculations. Figure B-1 shows a typical location of the assumed flaw on the OD of the nozzle.

Other parameters must be taken into account, such as the initial crack depth, the initial a/c ratio, and a possible change of a/c as the crack grows. Calculations start with a crack depth of 0.04 inches (1.0 mm) as was the case for the axial ID flaw growth calculations. Stress intensity factor coefficients at the surface of an axial OD flaw are provided in Table 3 and 4 of Reference (45) for crack aspect ratios (a/c) of 0.2, 0.4, and 1.0 ($a/2c$ from 1/10 to 1/2). It should be noted that for this flaw geometry, the influence coefficients G_j increase as the a/c ratio increases (ℓ/a

decreases), and the shape factor Q is also a function of a/c. Therefore, the calculations start with an initial a/c ratio of 1.0, which appears to be the most conservative case (this corresponds to assuming an initial length into the weld region of 0.04 inches). However, as the flaw grows toward the top of the weld, lower a/c ratios have been considered to simulate the growth in length and enable the crack to reach the top of the weld before its depth is through-wall (0.625 inches). In particular, the a/c ratio is conservatively assumed to decrease linearly from 1 to 1/3 at the point which the flaw becomes through-wall.

Figures B2-5 through B2-8.b show the stress intensity factors calculated for the stress distributions in Figures B2-1 through B2-4.b, respectively.

b. Crack Growth Rate Calculation Method

The crack growth rate in Alloy 600 nozzle material is computed using the method specified in the current NRC guidance (7) as reported in paragraph B.1.

The results of the crack growth calculations for OD axial flaws are shown in Figures B2-9 through B2-12.b, and the summary results of Table B-1. These figures show the flaw half length into the weld region (c) as a function of time computed using the crack tip stress intensity factors in Figures B2-5 through B2-8.b and the crack growth equation defined above. The curves can be compared to the location of the top of the weld, which gives the time for an OD axial crack starting at the bottom of the weld to reach the top of the weld and create a leak path.

B.3 Surface Weld Flaw

Calculations were performed as described in paragraph 7.2 for the four representative penetration geometries (0.0°, 9.3°, 27.1° and 46.0°) and the uphill and the downhill sides, with an initial flaw depth of 0.105 inches (2.67 mm). The results are shown in Figures B3-1.a and B3-1.b. As described in paragraph 7.2, the limit of detectability is taken as 0.16 inches (4.1 mm) length, and a typical weld flaw length to depth aspect ratio of 1.5:1 is assumed (25, 57), resulting in an initial depth assumption of 0.105 inches (2.67 mm) for the calculations shown in Figures B3-1.a and B3-1.b. These results were used as an input to the probabilistic evaluation of Section 8.

B.4 Through-Wall Circumferential Flaw in Nozzle

Calculations were performed to determine the time for a 30° through-wall circumferential crack above the J-groove weld to grow to the limit flaw arc length of 284° as calculated in Appendix E using a safety factor of 2.7 on the design pressure, and also to 300° for the probabilistic evaluation in Section 8. The final arc length of 300° for the probabilistic calculations is the greatest angle for which the most applicable stress intensity factor results were available, and it is conservative to model nozzle ejection at a crack size of 300° because the critical flaw size at a pressure loading of 2500 psi is 330°. Figure B4-3 shows the growth of a through-wall circumferential flaw around the nozzle circumference.

Independent calculations of the crack tip stress intensity factor for through-wall circumferential flaws were not performed as part of this effort. Rather, the crack tip stress

intensity factor was established based on other work performed in the industry. Figure B4-1 shows several sources of reported crack tip stress intensity factors for through-wall circumferential cracks above the J-groove weld. The sources of data are as follows:

- The "Westinghouse" curve is from WCAP-15928 (47). This curve was not calculated by Westinghouse, but is reported to represent a composite of other reported data.

- The "EMC^2" curve was reported by Dr. Shack of Argonne National Laboratory in October 2002 (48). It is reported to represent analyses by Engineering Mechanics Corporation of Columbus on behalf of the NRC.

- The "MRP" curves were developed by the EPRI Materials Reliability Program based on elastic-plastic finite element analyses performed for an outer row Westinghouse plant CRDM penetration that has a very similar weld geometry to Robinson (both weld size and uphill vs. downhill side distribution) and a high yield strength (8, 57). These data were presented to the NRC on June 12, 2003. These stress intensity factors were conservatively calculated based on "enveloping stresses" perpendicular to the crack plane that correspond to a meandering crack plane through the highest stress locations above the weld. In other words, the circumferential crack is assumed to move to the elevation having the highest stress perpendicular to the crack plane as the crack progresses around the circumference.

- The "Center Cracked Panel" curve represents a central through-wall crack in an axially loaded panel. While not believed to provide meaningful results for small flaws due to the lack of residual stresses, it is believed to be accurate for large flaws where residual stresses have largely been relieved.

Based on the above data, the MRP stress intensity factor curves (8, 57)—which are tabulated in Tables B4-1.a and B4-1.b—were chosen for application to Robinson. The results of the crack growth calculations for eight representative through-wall circumferential flaw geometries are shown in Figures B4-2.a and B4-2.b. Note that the results for circumferential flaws originating on the uphill side (Figure B4-2.a) all assume the same stress intensity factor curve that was calculated for an "uphill" crack in an outer row penetration (49°). Similarly, the "downhill" results (Figure B4-2.b) are all based on one stress intensity factor curve. In each case, the stress intensity factor curve used is conservative since the magnitude of the calculated stresses increases with increasing nozzle angle. The source of the differences between the curves in each figure is that each circumferential flaw is assumed to follow the weld contour so that the actual crack growth distance is greatest for the 46° nozzle angle cases. Finally, note that the average of the nozzle OD and ID (3.375") was used to determine the crack growth distance (3.7" on each crack front for growth from 30° to 284°), and that growth is assumed to take place on both crack fronts at the same time.

As was mentioned in Section 7, the deterministic calculation of circumferential crack growth includes a multiplicative factor of 2 increasing the MRP-55 (35) crack growth rate for Alloy 600 base metal to account for current uncertainties in the exact chemical environment that exists in the nozzle OD annulus for a leaking penetration. This factor is recommended by MRP-55 and reflected in Figures B4-2.a and B4-2.b and the summary results of Table B-1. However, as discussed in paragraph 8.2, the probabilistic calculations of Section 8 do not include this factor of 2 on crack growth rate.

B.5 Evaluation of Circumferential Cracking Initiating at Multiple Initiation Sites

Calculations were performed to assess the influence of potential crack growth in the radial direction from multiple initiation sites on the nozzle OD. Figures B5-1 and B5-2 show the through-wall distribution of the stress perpendicular to the circumferential crack plane (for the outermost Robinson penetration geometry) at the top of the weld, one element row above, and two element rows above the top of the weld, based on the C-3515-00-1 stress model of Appendix A. The heavier lines in Figure B5-2 show the stresses in the region between the uphill and downhill sides of the nozzle, i.e., in the region of the 90°/270° azimuthal position.

Stress intensity factors were calculated at the deepest point of a part-depth OD circumferential crack based on the Raju-Newman solution for a flat plate and a cubic stress distribution assuming an aspect ratio of $2c/a = 6$ (Figure B5-3). The crack face was conservatively assumed to be pressurized at the internal vessel pressure. Stress intensity factors were also calculated based on the ASME Section XI, article A-3000(a) (61) flat plate solution for a cubic stress distribution assuming an aspect ratio of $2c/a = 6$ (Figure B5-4). The crack face was assumed to be pressurized, and surface correction factors were extrapolated from the tables for a/t ratios greater than 0.8. Note that the A-3000(a) solution includes a correction factor for the size of the plastic zone at the crack tip.

These results show that the calculated time for growth of a through-wall circumferential crack around the nozzle circumference bounds the effect of potential crack growth in the radial direction from multiple initiation sites on the nozzle OD following formation of a leak path flaw to the OD annulus. The difference in stress intensity factor between that assumed for circumferential growth of a through-wall circumferential flaw ("downhill" MRP curve in Figure B4-1) and that calculated in Figures B5-3 and B5-4 for a part-depth circumferential flaw are large enough so that less time is required for the through-wall crack to grow all the way around the nozzle than for a part-depth crack located between the uphill and downhill positions to grow through the entire wall thickness. This is true even if one does not take credit for the apparent stress intensity factor threshold of Equation B-5, for example, by just assuming a linear dependence of crack growth rate on stress intensity factor. Moreover, some significant time would be expected for the part-depth circumferential cracks to initiate—i.e., reach the SCC growth phase—after the time that a leak path flaw to the nozzle OD annulus first forms.

Table B-1
Summary of the Deterministic Crack Growth Calculations

ID Axial Flaw (Time to Leak)		
Angle (°)	UH/DH	Time (yrs)
0.0	--	4.8
9.3	UH	4.9
9.3	DH	4.3
27.1	UH	5.1
27.1	DH	3.5
46.0	UH	4.9
46.0	DH	3.5

Min	*3.5*
Max	*5.1*

OD Axial Flaw (Time to Leak)		
Angle (°)	UH/DH	Time (yrs)
0.0	--	9.5
9.3	UH	8.0
9.3	DH	8.6
27.1	UH	7.4
27.1	DH	5.4
46.0	UH	10.0
46.0	DH	7.1

Min	*5.4*
Max	*10.0*

OD Circ. Flaw (30° to 300°)		
Angle (°)	UH/DH	Time (yrs)
0.0	UH	49.9
0.0	DH	7.5
9.3	UH	50.6
9.3	DH	7.6
27.1	UH	56.1
27.1	DH	8.4
46.0	UH	71.9
46.0	DH	10.8

Min	*7.5*
Max	*71.9*

Table B4-1.a
Stress Intensity Factors for OD Circumferential Cracks (Downhill Side) (8, 57)

Total Flaw Angle (°)	*K (ksi √in)*	*K (MPa √m)*
30	28.790	31.636
90	59.336	65.201
160	84.080	92.390
180	86.557	95.112
220	89.310	98.137
260	92.769	101.938
300	93.453	102.690

Table B4-1.b
Stress Intensity Factors for OD Circumferential Cracks (Uphill Side) (8, 57)

Total Flaw Angle (°)	*K (ksi √in)*	*K (MPa √m)*
30	4.942*	5.430*
90	14.302	15.716
160	21.782	23.935
180	24.115	26.499
220	30.100	33.075
260	38.017	41.775
300	50.009	54.952

* Values changed to 14.302 and 15.716

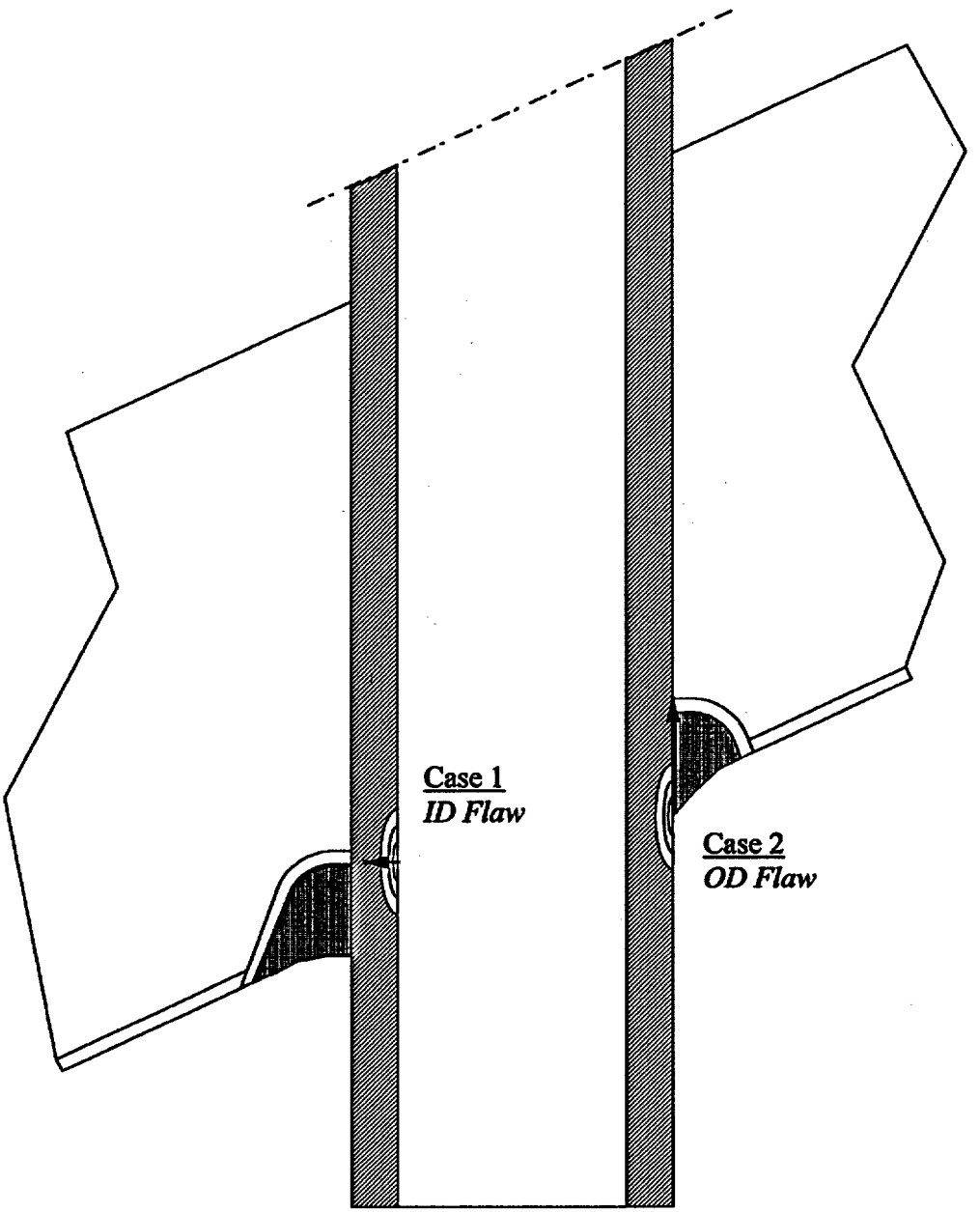

Figure B-1
Example of ID and OD Flaw Locations.

Confidential Commercial Information

Figure B1-1 - Through-Wall Hoop Stress Distribution at Controlling Elevation - 0.0° Nozzle

Confidential Commercial Information

Figure B1-2.a - Through-Wall Hoop Stress Distribution at Controlling Elevation - 9.3° Nozzle - Uphill Side

Confidential Commercial Information

Figure B1-2.b - Through-Wall Hoop Stress Distribution at Controlling Elevation - 9.3° Nozzle - Downhill Side

Confidential Commercial Information

Figure B1-3.a - Through-Wall Hoop Stress Distribution at Controlling Elevation – 27.1° Nozzle - Uphill Side

Confidential Commercial Information

Figure B1-3.b - Through-Wall Hoop Stress Distribution at Controlling Elevation – 27.1° Nozzle - Downhill Side

Confidential Commercial Information

Figure B1-4.a - Through-Wall Hoop Stress Distribution at Controlling Elevation – 46.0° Nozzle - Uphill Side

Confidential Commercial Information

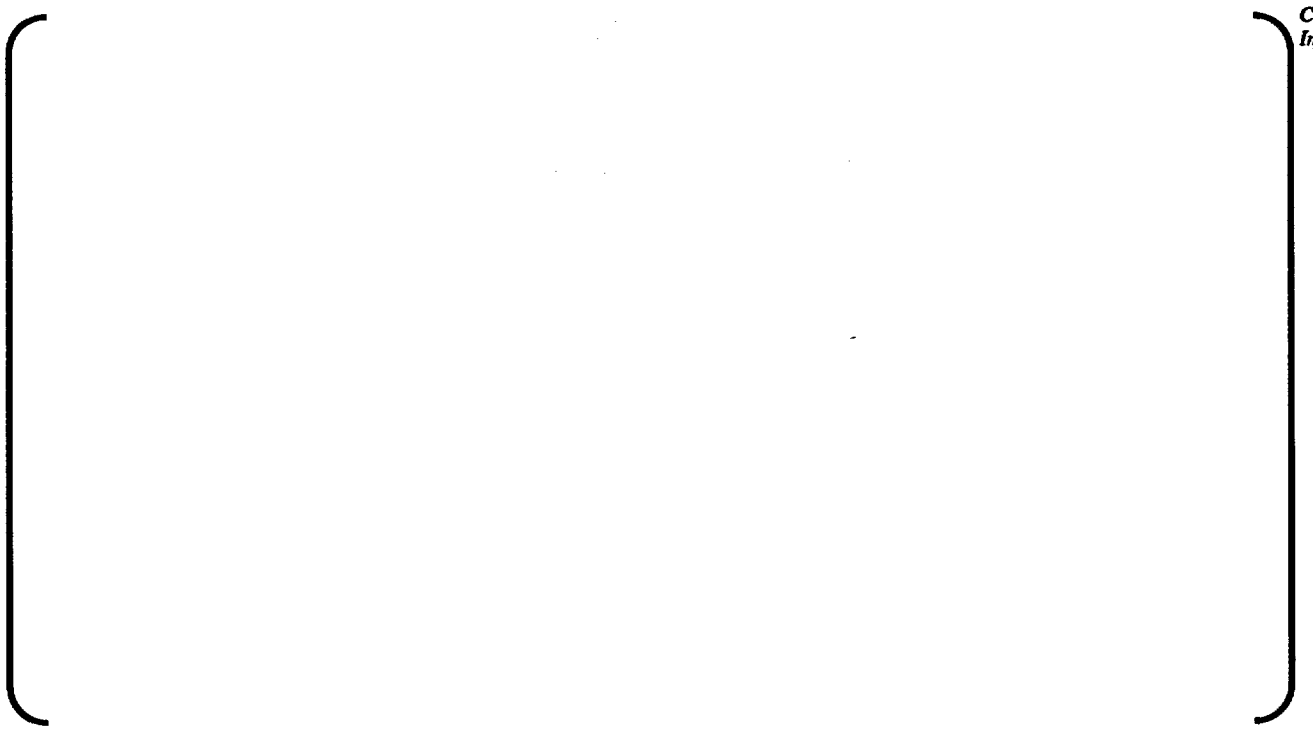

Figure B1-4.b - Through-Wall Hoop Stress Distribution at Controlling Elevation – 46.0° Nozzle - Downhill Side

Confidential Commercial Information

Figure B1-5 - Through-Wall Stress Intensity Factor Distribution - 0.0° Nozzle

Confidential Commercial Information

Figure B1-6.a - Through-Wall Stress Intensity Factor Distribution – 9.3° Nozzle - Uphill Side

Confidential Commercial Information

Figure B1-6.b - Through-Wall Stress Intensity Factor Distribution – 9.3° Nozzle - Downhill Side

Confidential Commercial Information

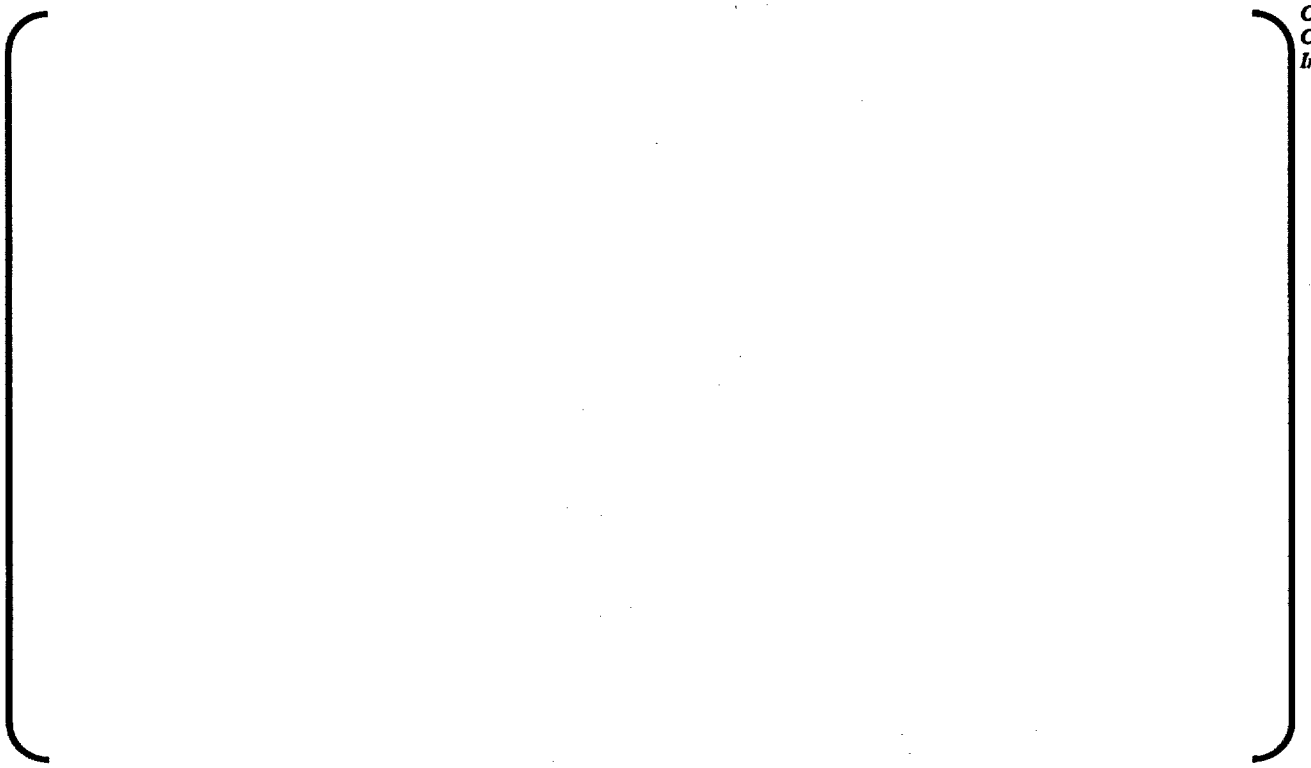

Figure B1-7.a - Through-Wall Stress Intensity Factor Distribution – 27.1° Nozzle - Uphill Side

Confidential Commercial Information

Figure B1-7.b - Through-Wall Stress Intensity Factor Distribution - 27.1° Nozzle - Downhill Side

Confidential Commercial Information

Figure B1-8.a - Through-Wall Stress Intensity Factor Distribution - 46.0° Nozzle - Uphill Side

Confidential Commercial Information

Figure B1-8.b - Through-Wall Stress Intensity Factor Distribution - 46.0° Nozzle - Downhill Side

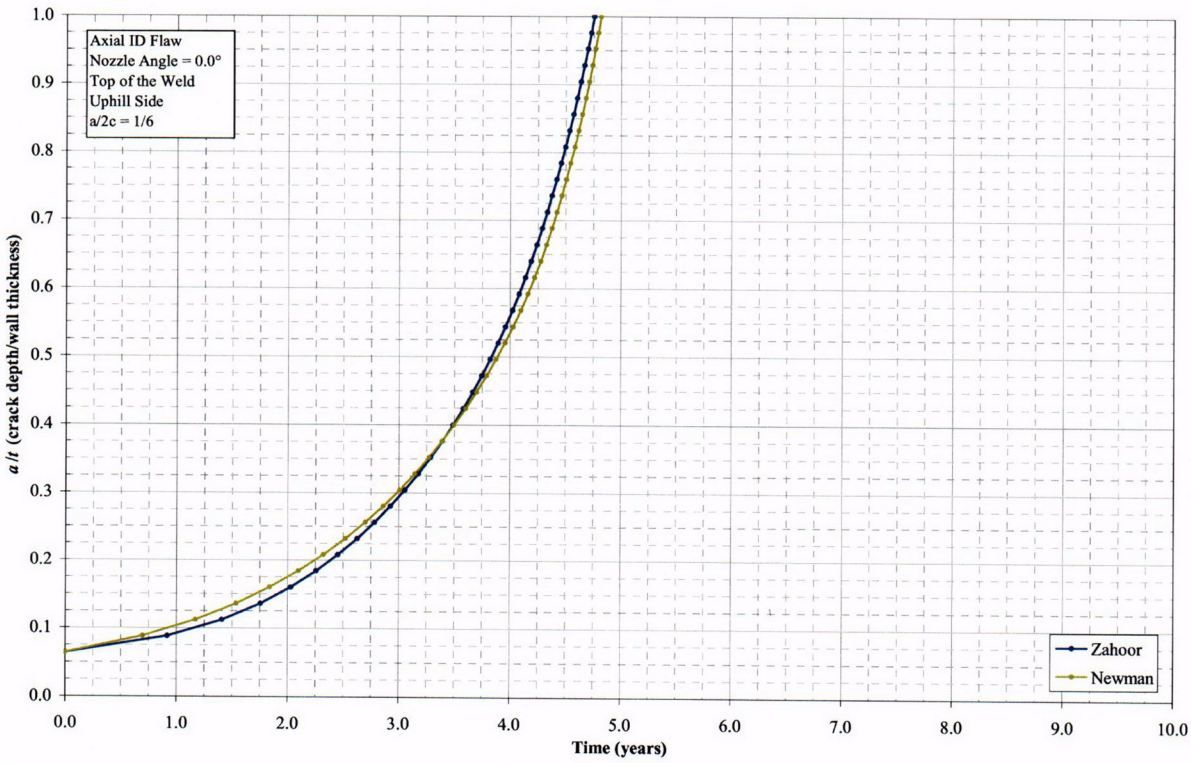

Figure B1-9 - Crack Growth Time for ID Axial Flaws - 0.0° Nozzle

C10

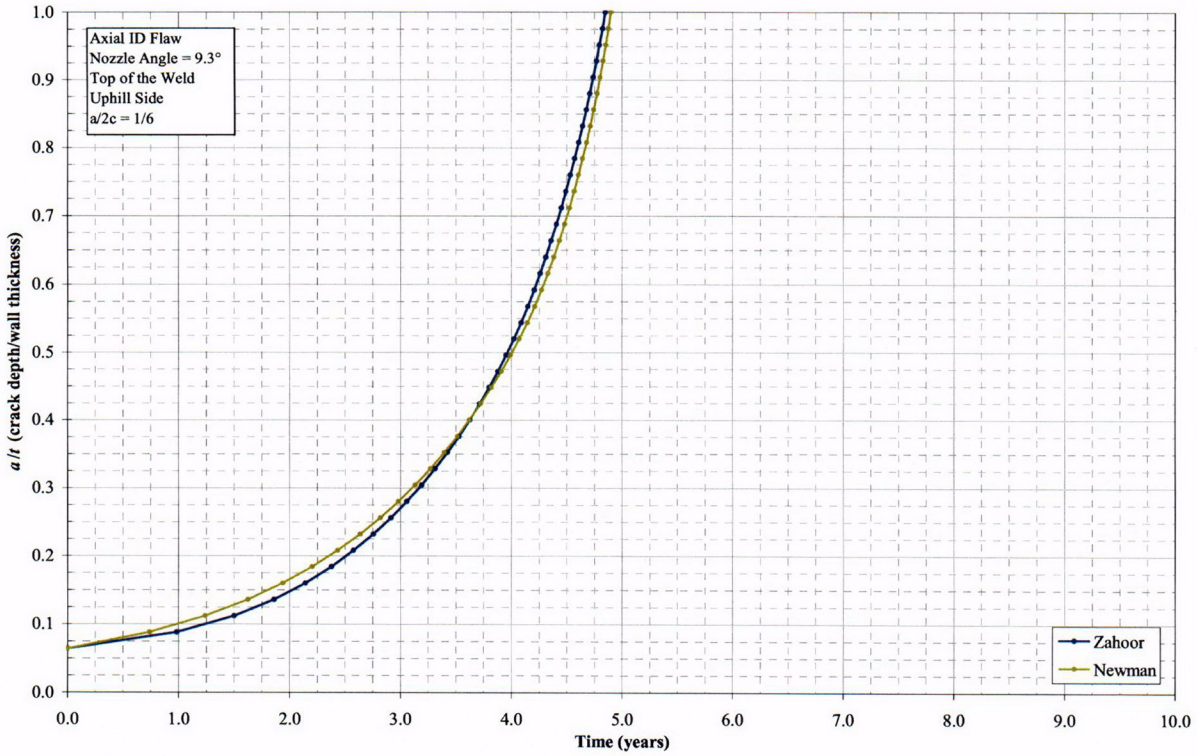

Figure B1-10.a - Crack Growth Time for ID Axial Flaws – 9.3° Nozzle - Uphill Side

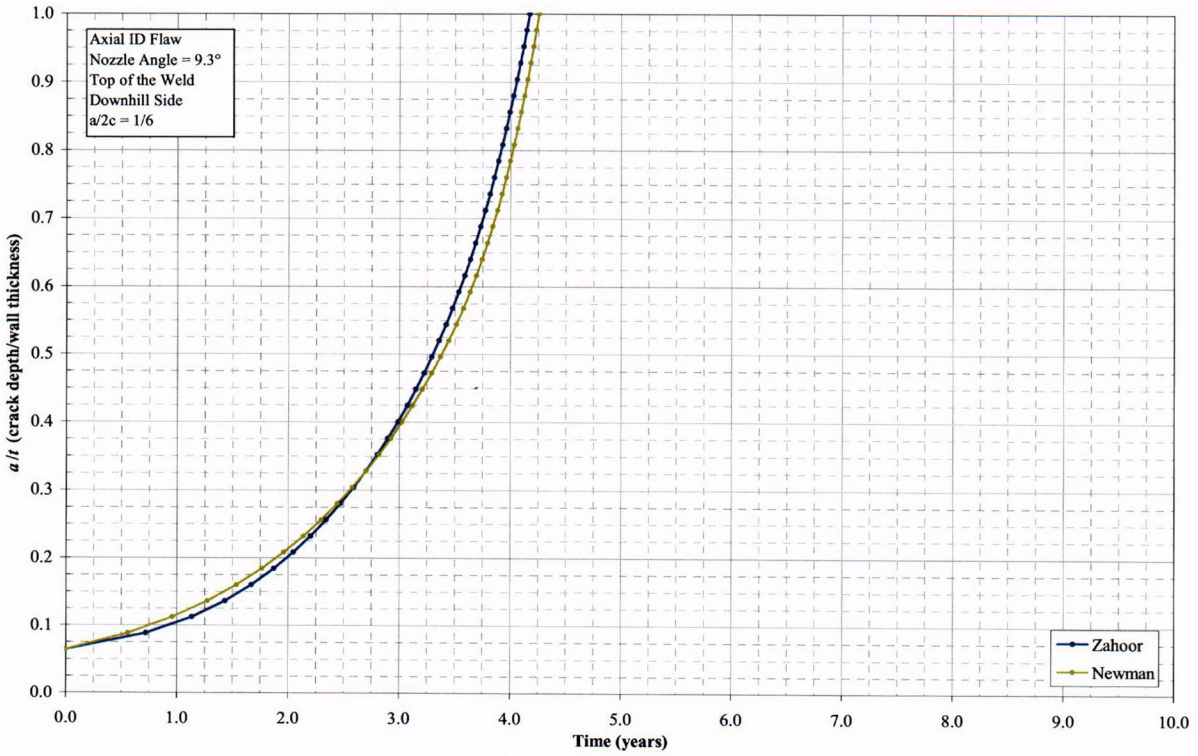

Figure B1-10.b - Crack Growth Time for ID Axial Flaws – 9.3° Nozzle - Downhill Side

C11

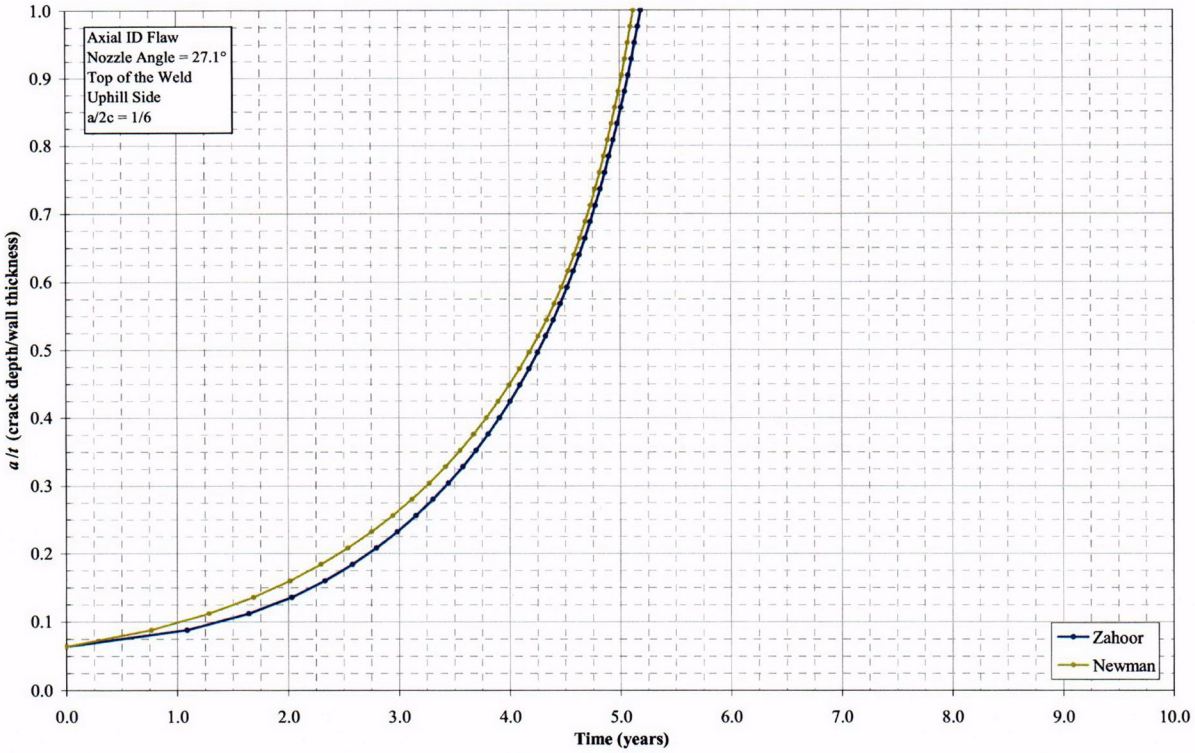

Figure B1-11.a - Crack Growth Time for ID Axial Flaws – 27.1° Nozzle - Uphill Side

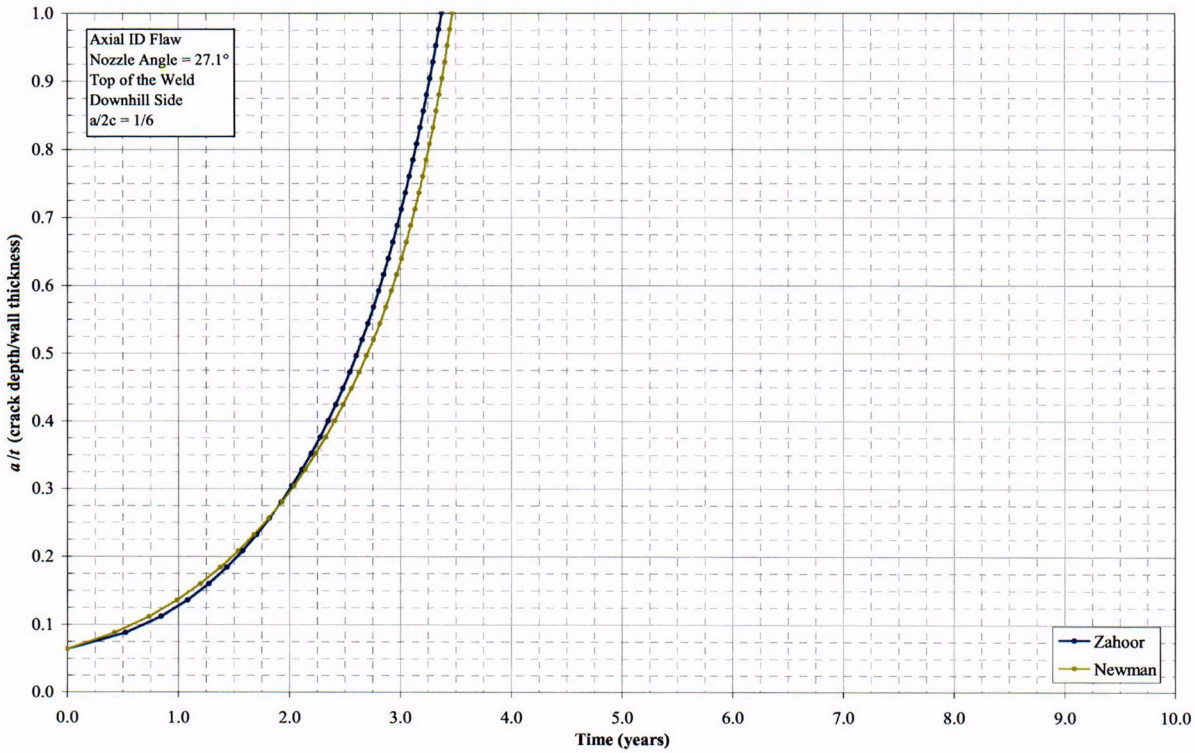

Figure B1-11.b - Crack Growth Time for ID Axial Flaws – 27.1° Nozzle - Downhill Side

C12

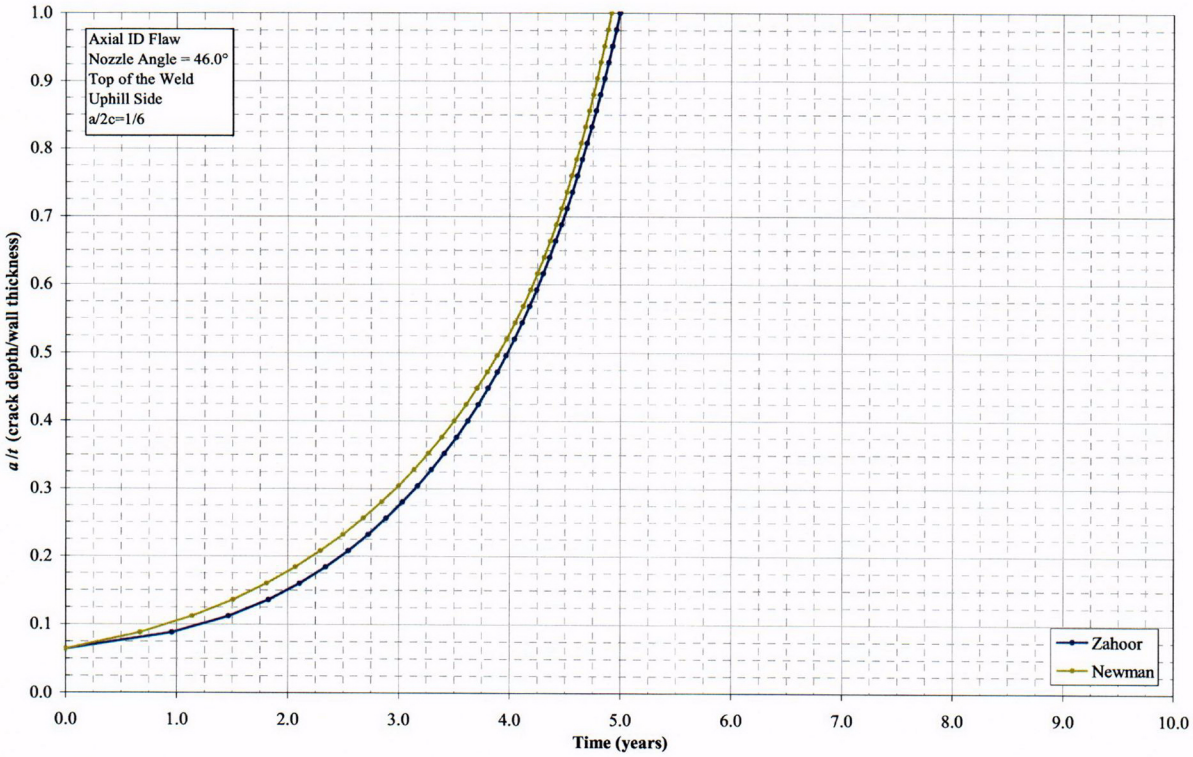

Figure B1-12.a - Crack Growth Time for ID Axial Flaws - 46.0° Nozzle - Uphill Side

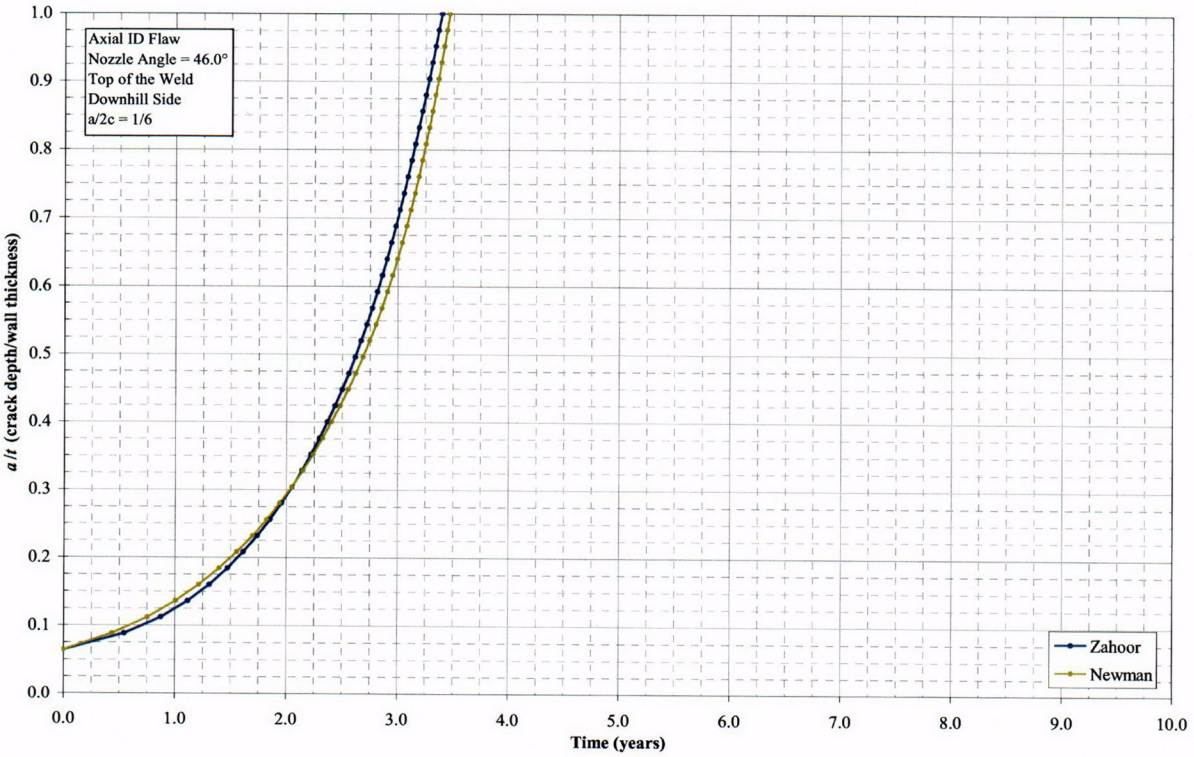

Figure B1-12.b - Crack Growth Time for ID Axial Flaws - 46.0° Nozzle - Downhill Side

Confidential Commercial Information

Figure B2-1 - Through-Wall Hoop Stress Distribution at the Bottom of the Weld - 0.0° Nozzle

Confidential Commercial Information

Figure B2-2.a - Through-Wall Hoop Stress Distribution at the Bottom of the Weld – 9.3° Nozzle - Uphill Side

Confidential Commercial Information

Figure B2-2.b - Through-Wall Hoop Stress Distribution at the Bottom of the Weld – 9.3° Nozzle - Downhill Side

Confidential Commercial Information

Figure B2-3.a - Through-Wall Hoop Stress Distribution at the Bottom of the Weld – 27.1° Nozzle - Uphill Side

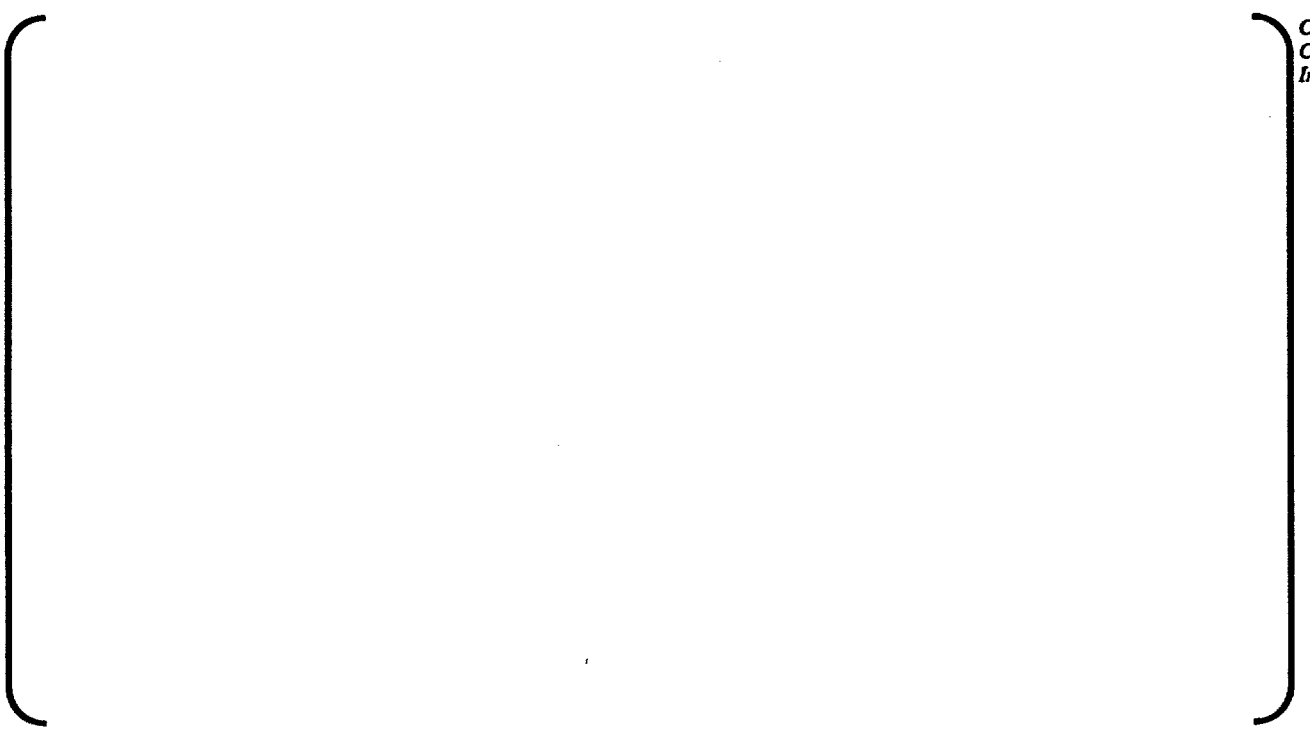

Confidential Commercial Information

Figure B2-3.b - Through-Wall Hoop Stress Distribution at the Bottom of the Weld – 27.1° Nozzle - Downhill Side

Confidential Commercial Information

Figure B2-4.a - Through-Wall Hoop Stress Distribution at the Bottom of the Weld - 46.0° Nozzle - Uphill Side

Confidential Commercial Information

Figure B2-4.b - Through-Wall Hoop Stress Distribution at the Bottom of the Weld - 46.0° Nozzle - Downhill Side

Confidential Commercial Information

Figure B2-5 - Stress Intensity Factor at OD Axial Flaw Upper Edge - 0.0° Nozzle

Confidential Commercial Information

Figure B2-6.a - Stress Intensity Factor at OD Axial Flaw Upper Edge – 9.3° Nozzle - Uphill Side

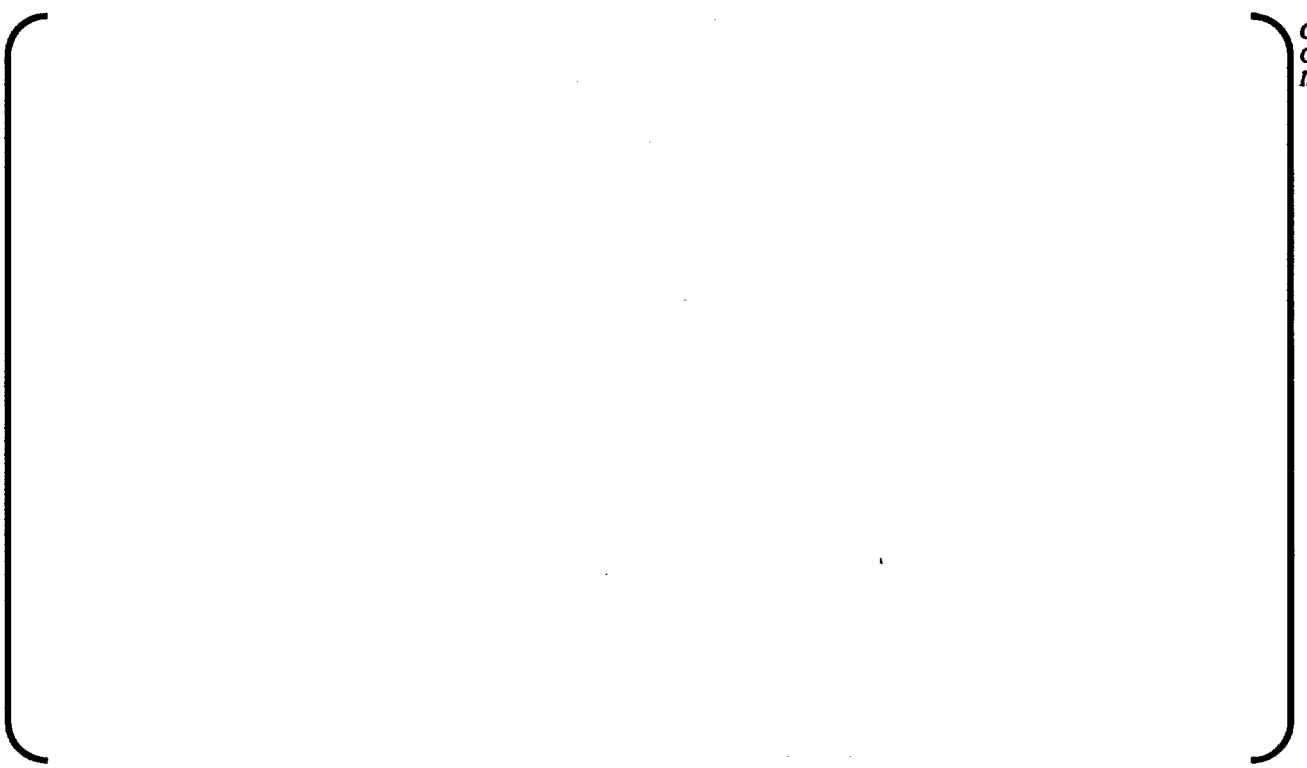

Confidential Commercial Information

Figure B2-6.b - Stress Intensity Factor at OD Axial Flaw Upper Edge – 9.3° Nozzle - Downhill Side

Confidential Commercial Information

Figure B2-7.a - Stress Intensity Factor at OD Axial Flaw Upper Edge – 27.1° Nozzle - Uphill Side

Confidential Commercial Information

Figure B2-7.b - Stress Intensity Factor at OD Axial Flaw Upper Edge – 27.1° Nozzle - Downhill Side

Confidential Commercial Information

Figure B2-8.a - Stress Intensity Factor at OD Axial Flaw Upper Edge - 46.0° Nozzle - Uphill Side

Confidential Commercial Information

Figure B2-8.b - Stress Intensity Factor at OD Axial Flaw Upper Edge - 46.0° Nozzle - Downhill Side

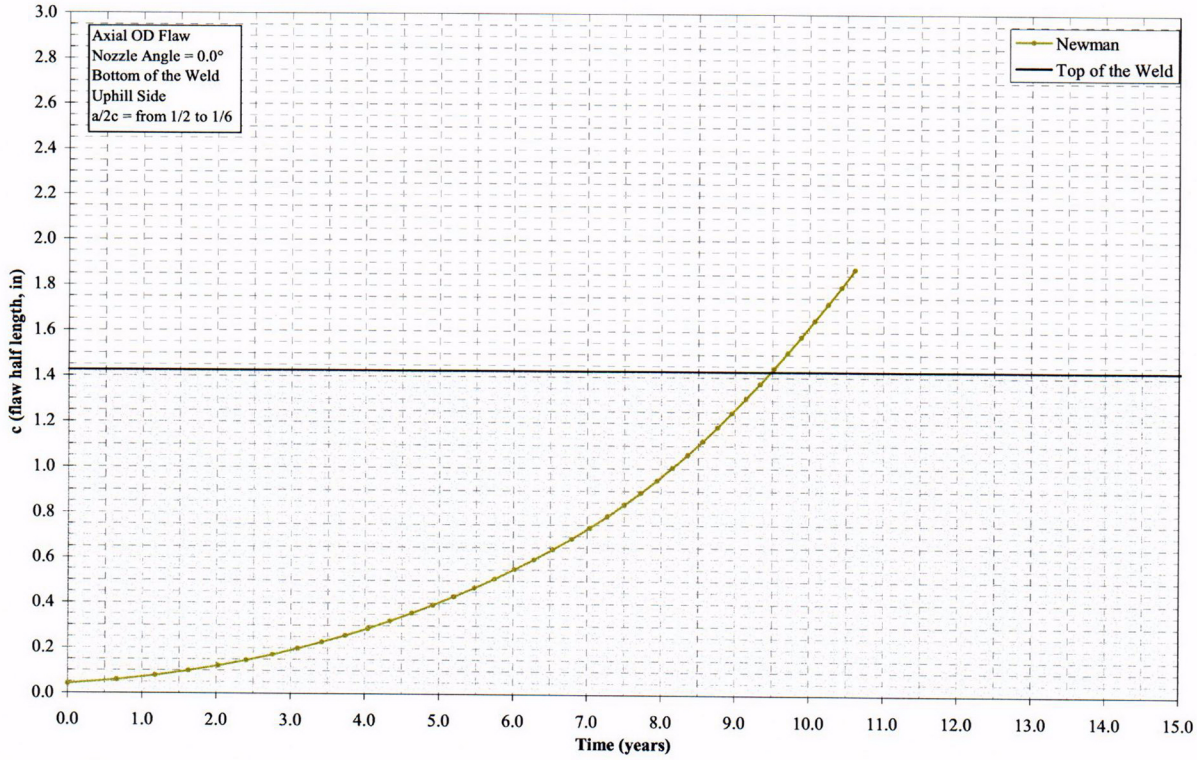

Figure B2-9 - Crack Growth Time of OD Axial Flaws - 0.0° Nozzle

C14

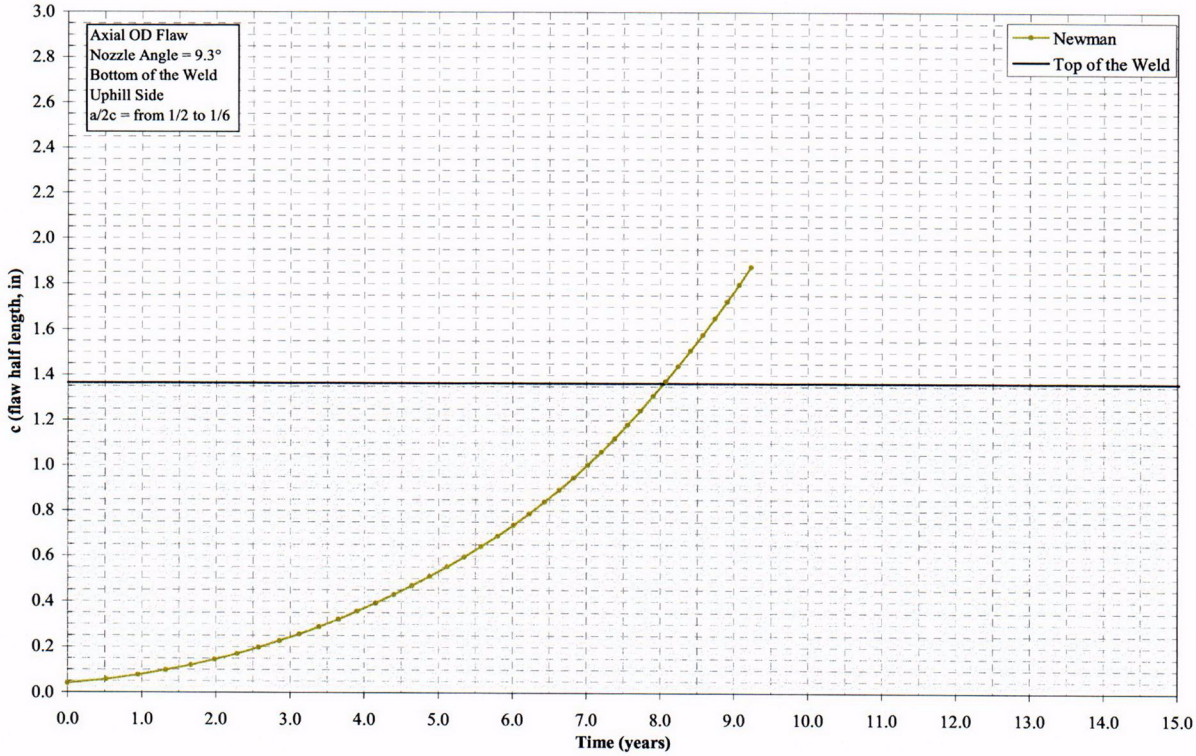

Figure B2-10.a - Crack Growth Time of OD Axial Flaws – 9.3° Nozzle - Uphill Side

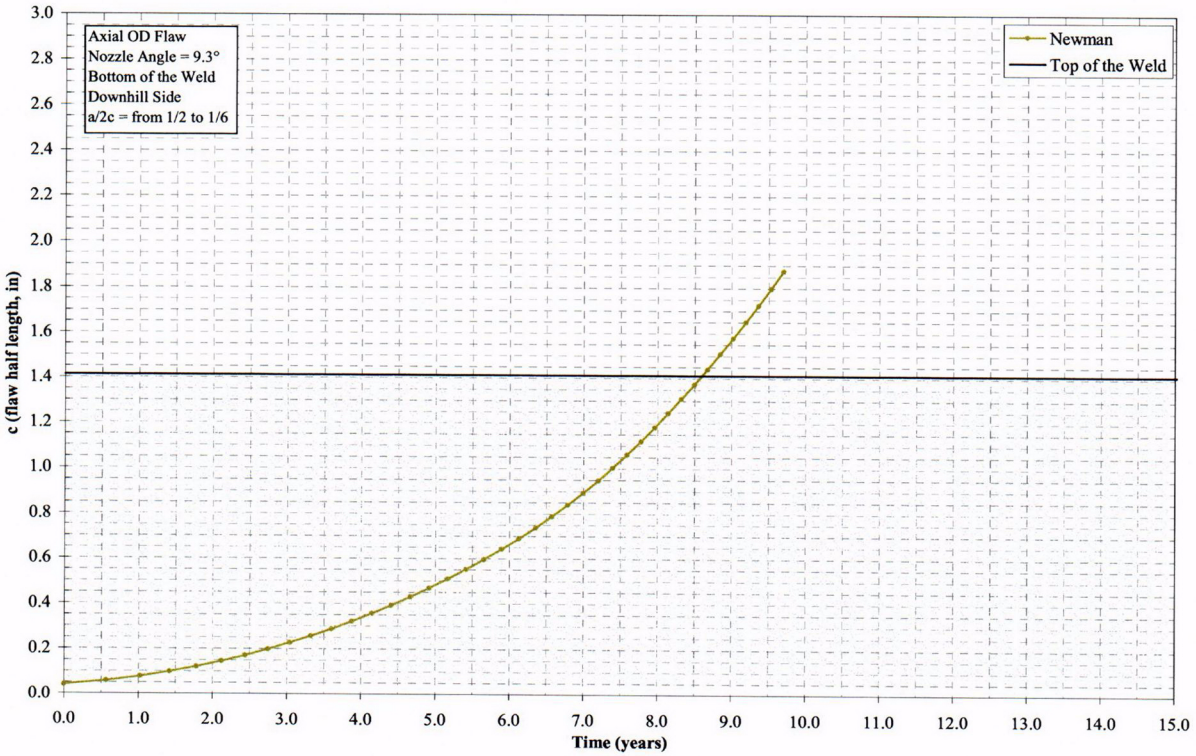

Figure B2-10.b - Crack Growth Time of OD Axial Flaws – 9.3° Nozzle - Downhill Side

C15

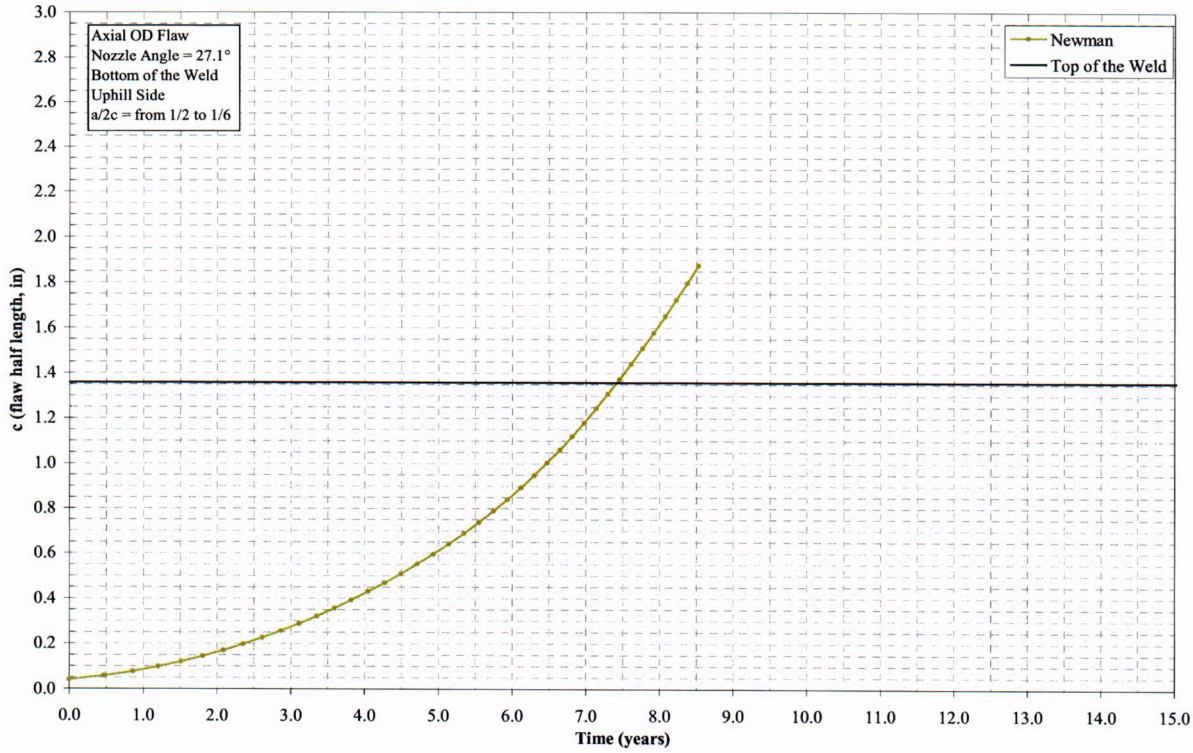

Figure B2-11.a - Crack Growth Time of OD Axial Flaws – 27.1° Nozzle - Uphill Side

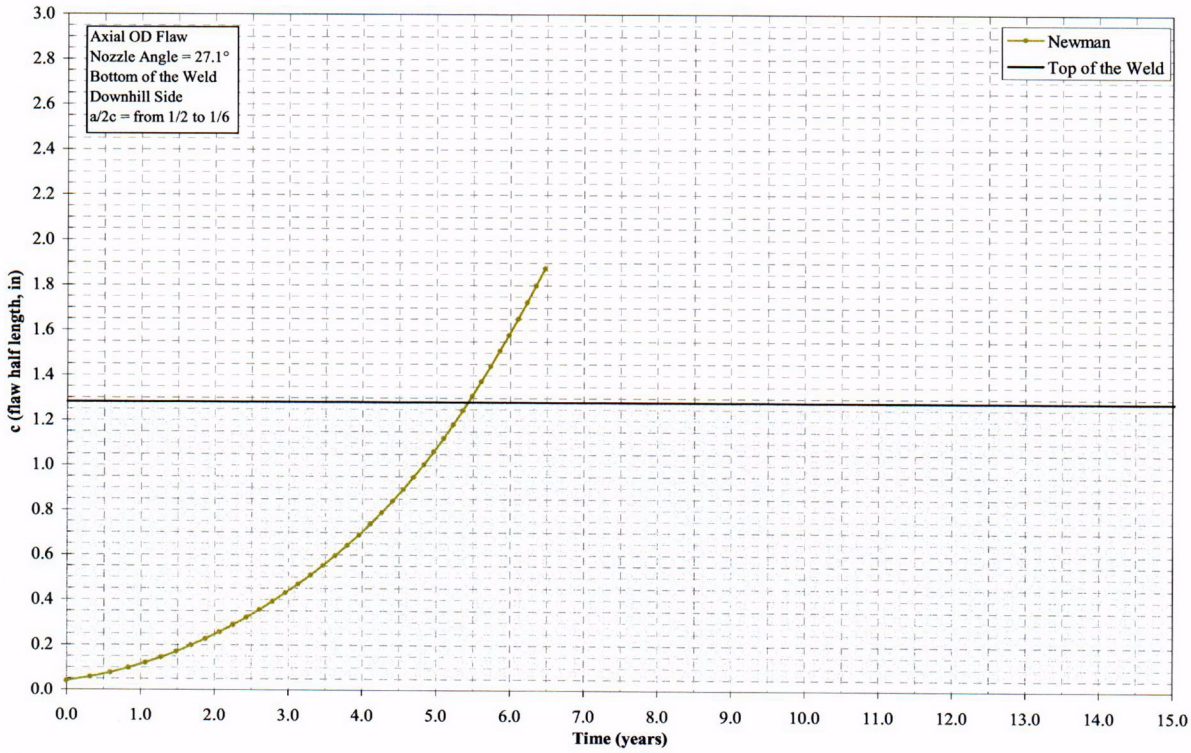

Figure B2-11.b - Crack Growth Time of OD Axial Flaws – 27.1° Nozzle - Downhill Side

C16

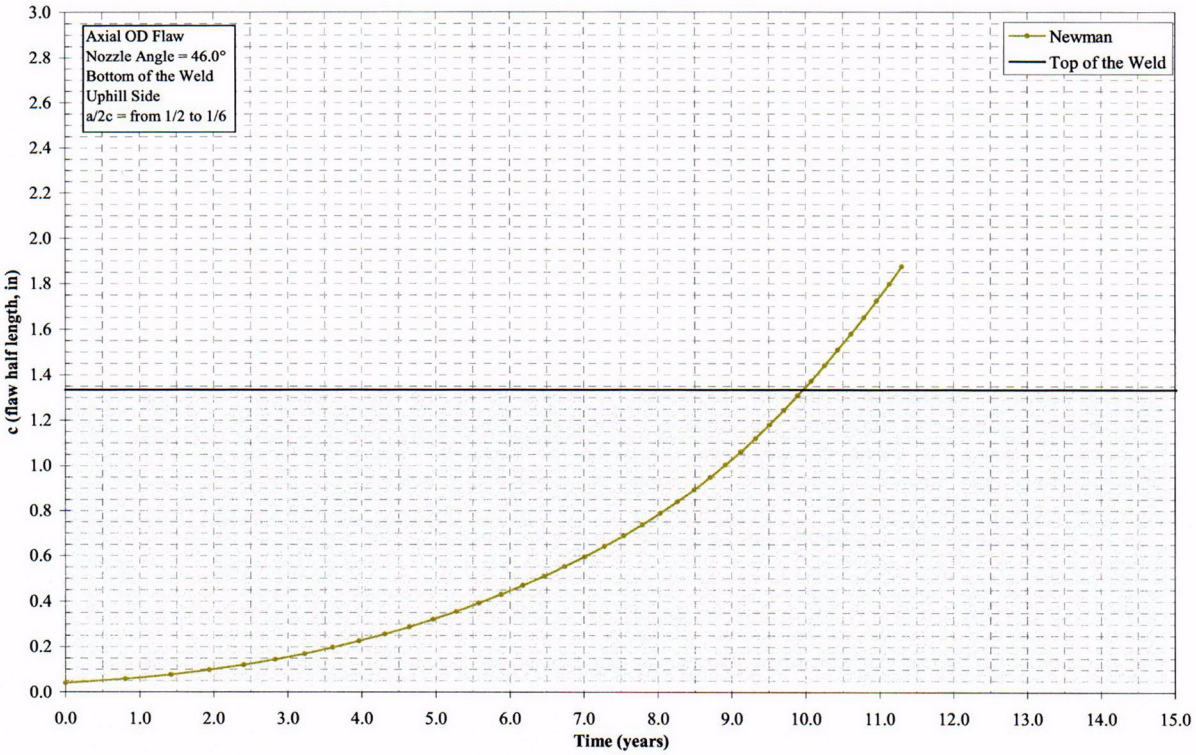

Figure B2-12.a - Crack Growth Time of OD Axial Flaws – 46.0° Nozzle - Uphill Side

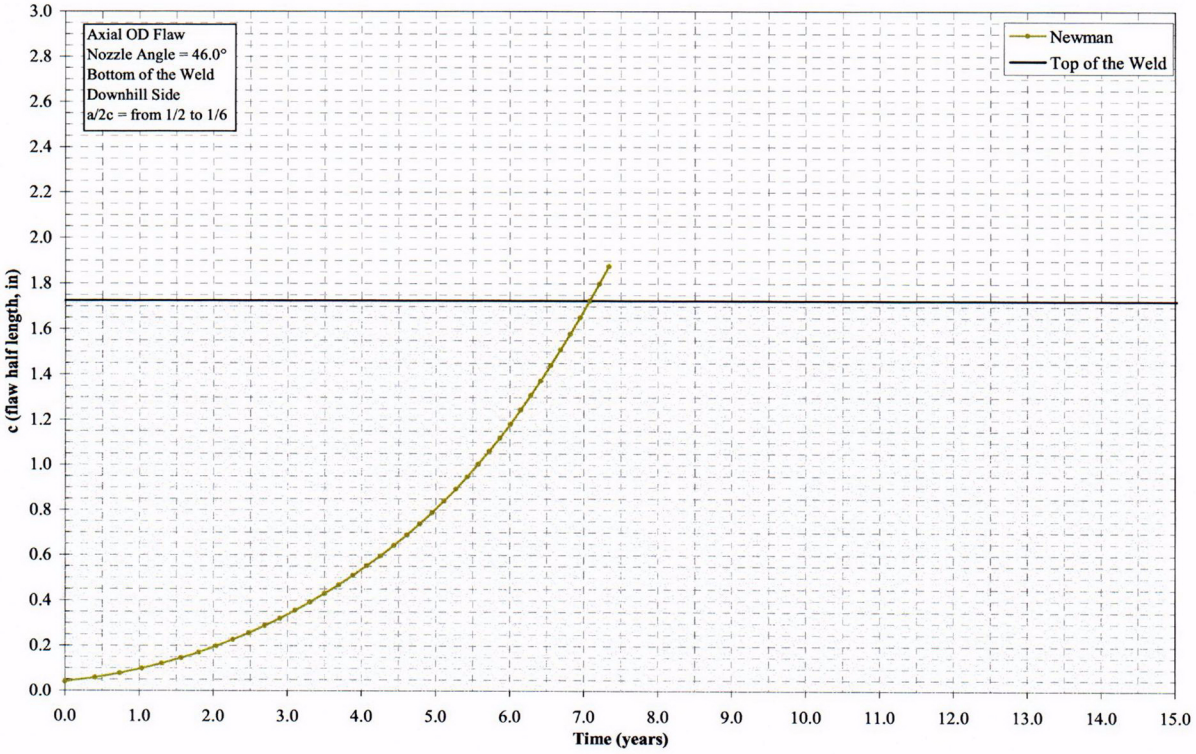

Figure B2-12.b - Crack Growth Time of OD Axial Flaws - 46.0° Nozzle - Downhill Side

C17

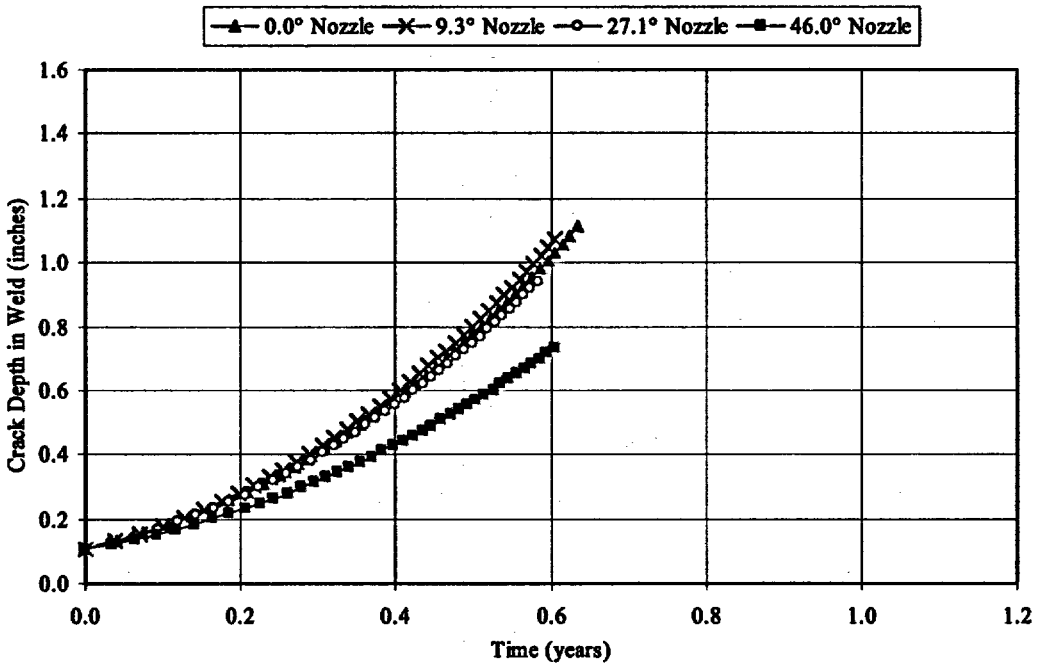

Figure B3-1.a
Predicted Crack Growth for Flaws in Weld (Uphill Side)

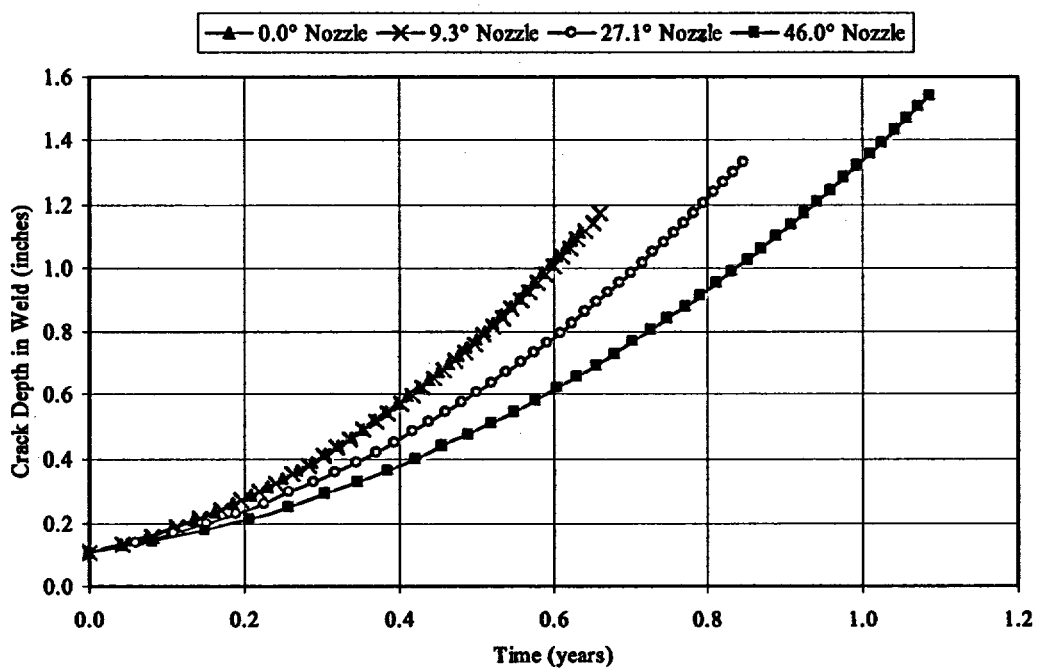

Figure B3-1.b
Predicted Crack Growth for Flaws in Weld (Downhill Side)

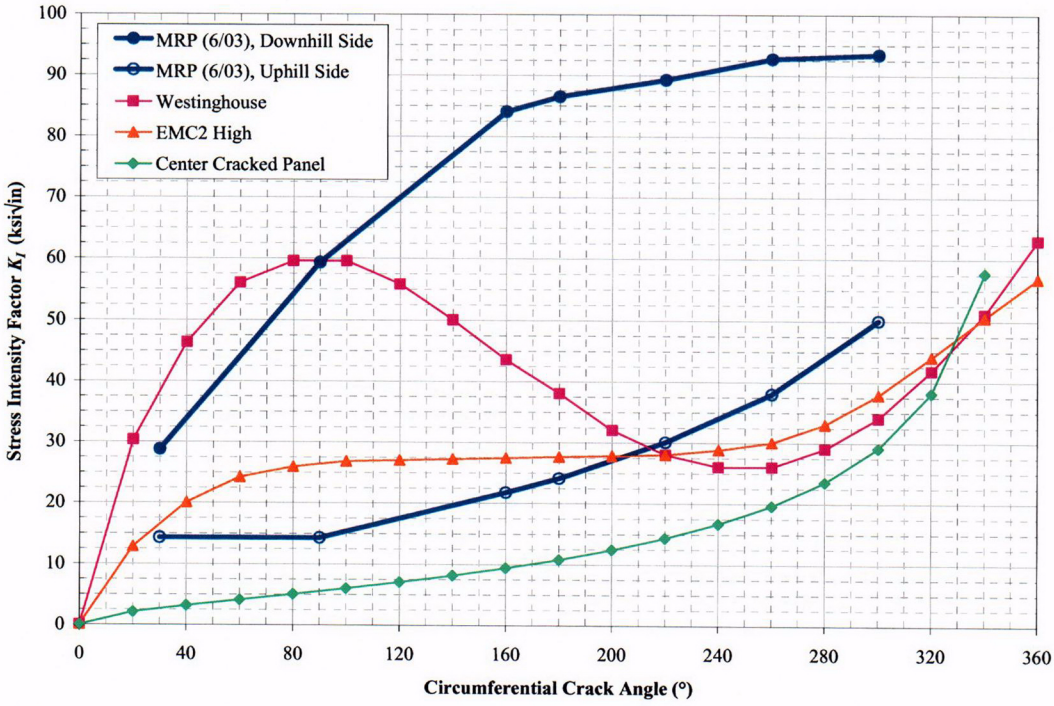

Figure B4-1
Stress Intensity for Through-Wall Circumferential Crack Above J-Groove Weld

C18

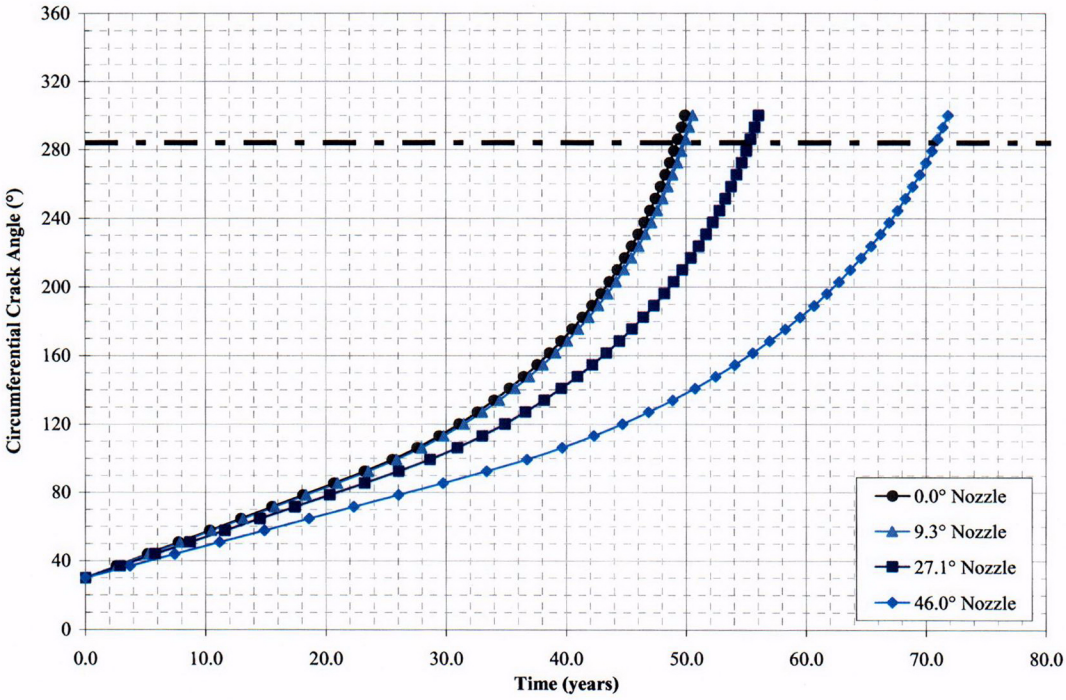

Figure B4-2.a
Growth of Circumferential Crack Above J-Groove Weld (Originating on the Uphill Side)

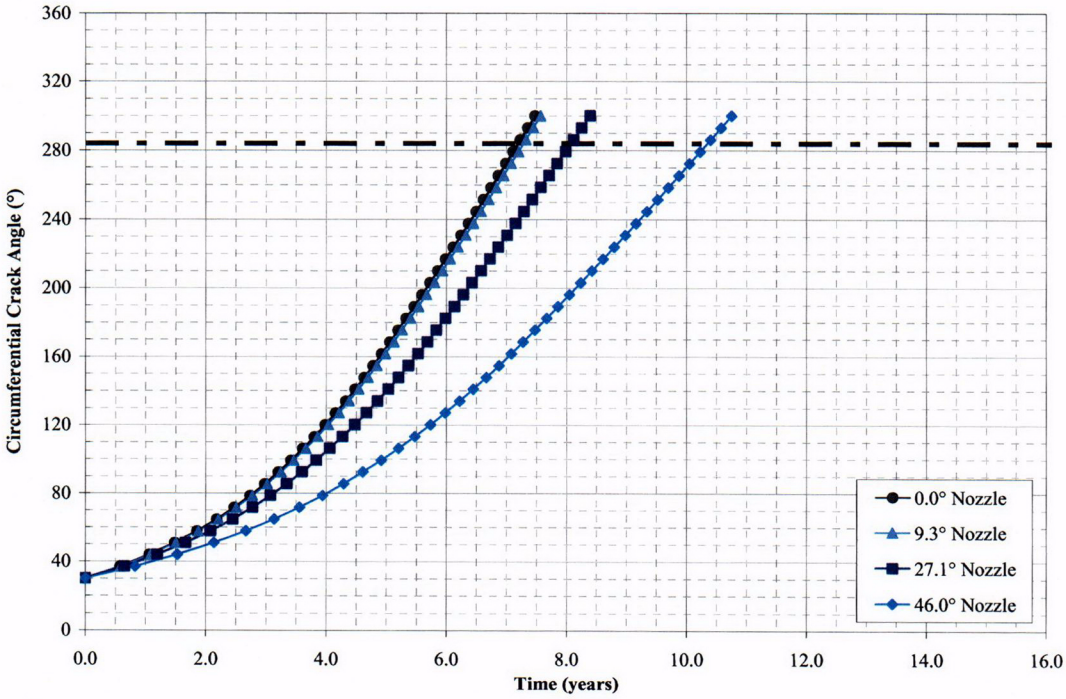

Figure B4-2.b
Growth of Circumferential Crack Above J-Groove Weld (Originating on the Downhill Side)

C19

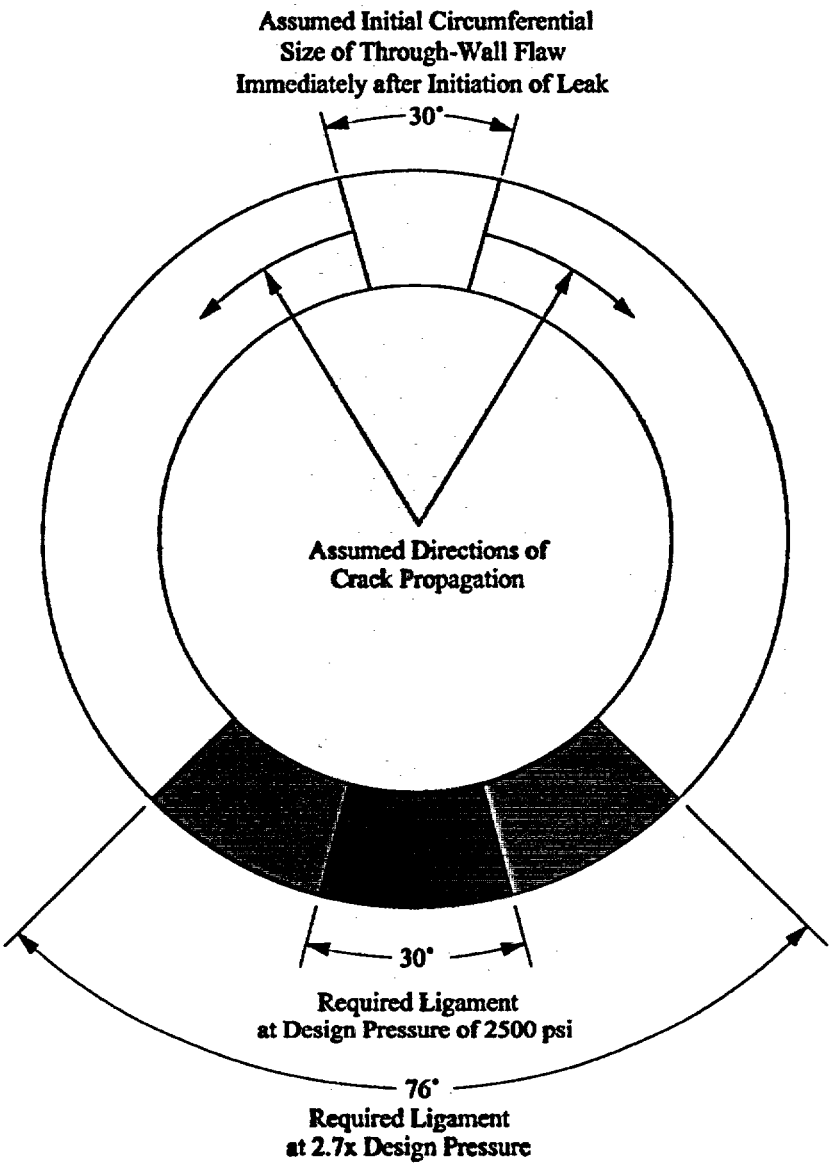

Figure B4-3
Growth of Above-Weld Circumferential Flaw Around the Nozzle Circumference

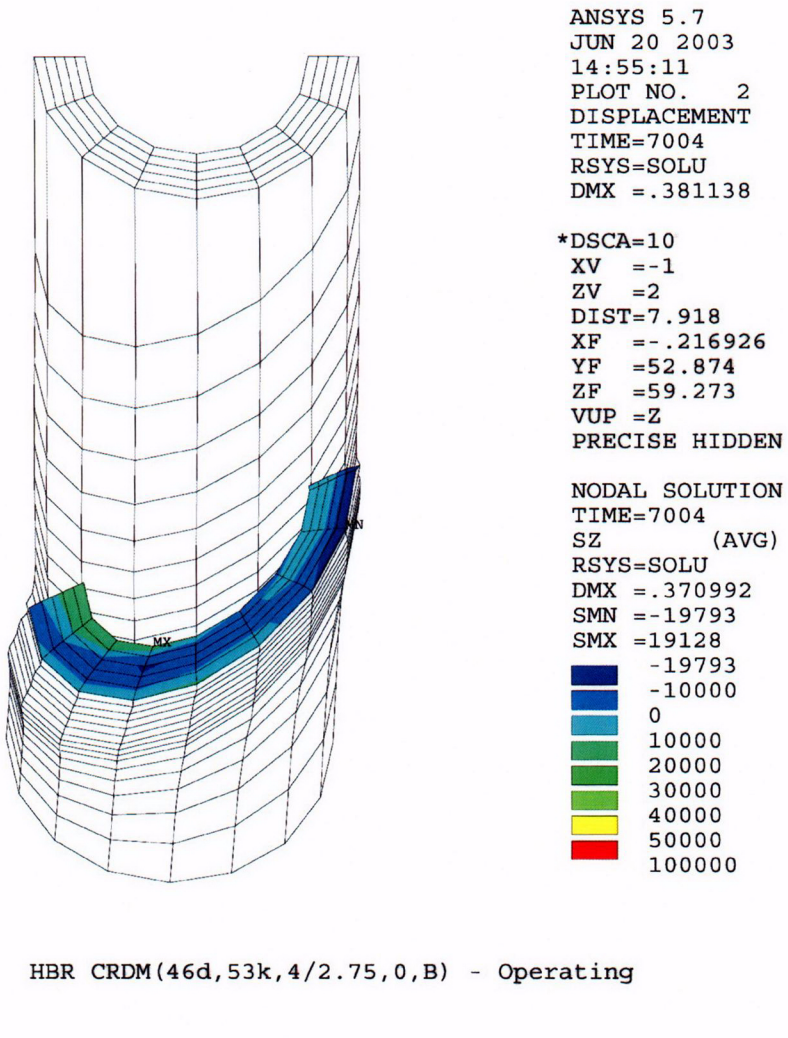

Figure B5-1
Contour Plot of the Stresses Perpendicular to the Crack Plane for the Outer Row

C20

Confidential Commercial Information

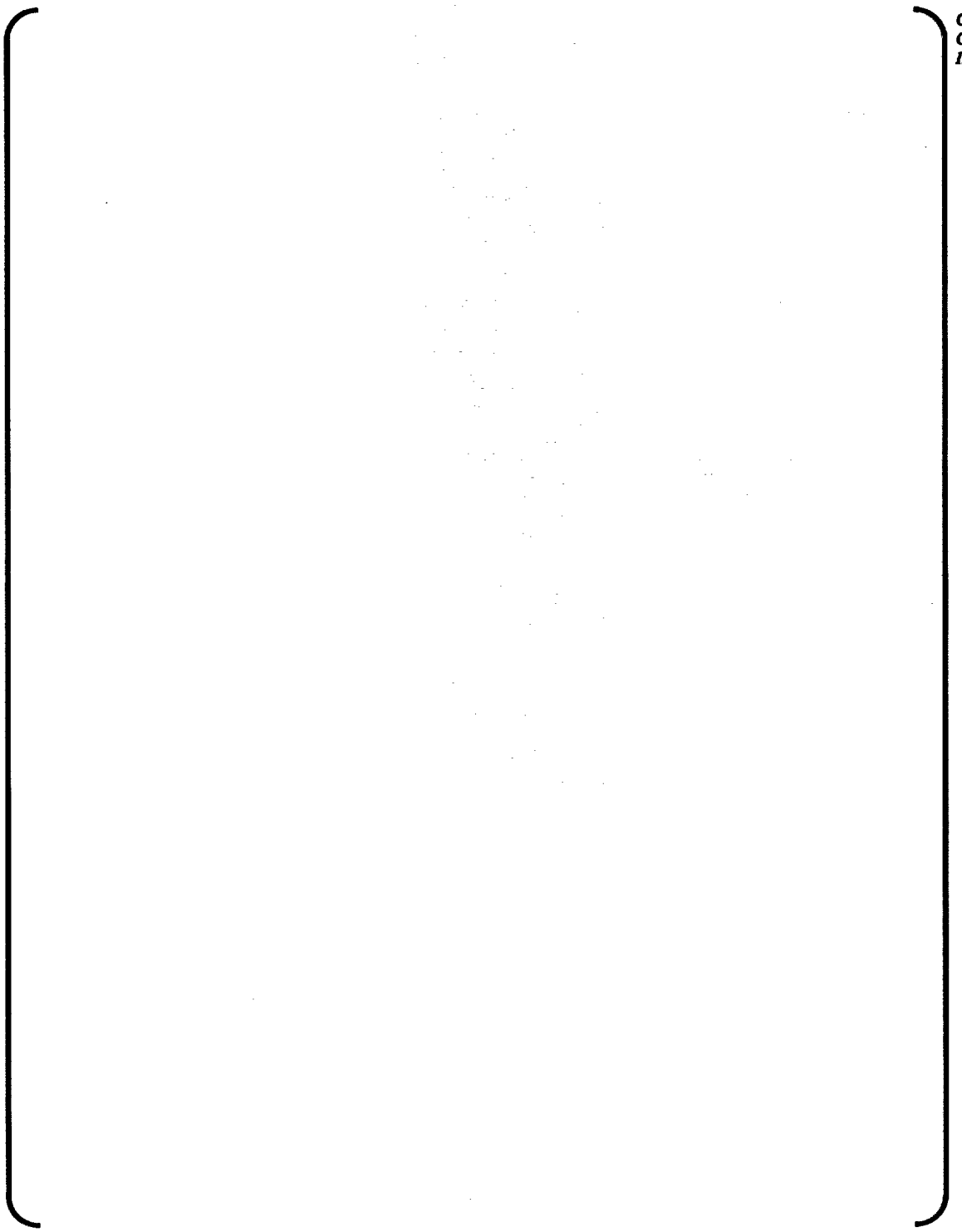

Figure B5-2
Stress Perpendicular to Plane of Circumferential Crack: (a) Top of Weld, (b) One Row Above and (c) Two Rows Above

Confidential Commercial Information

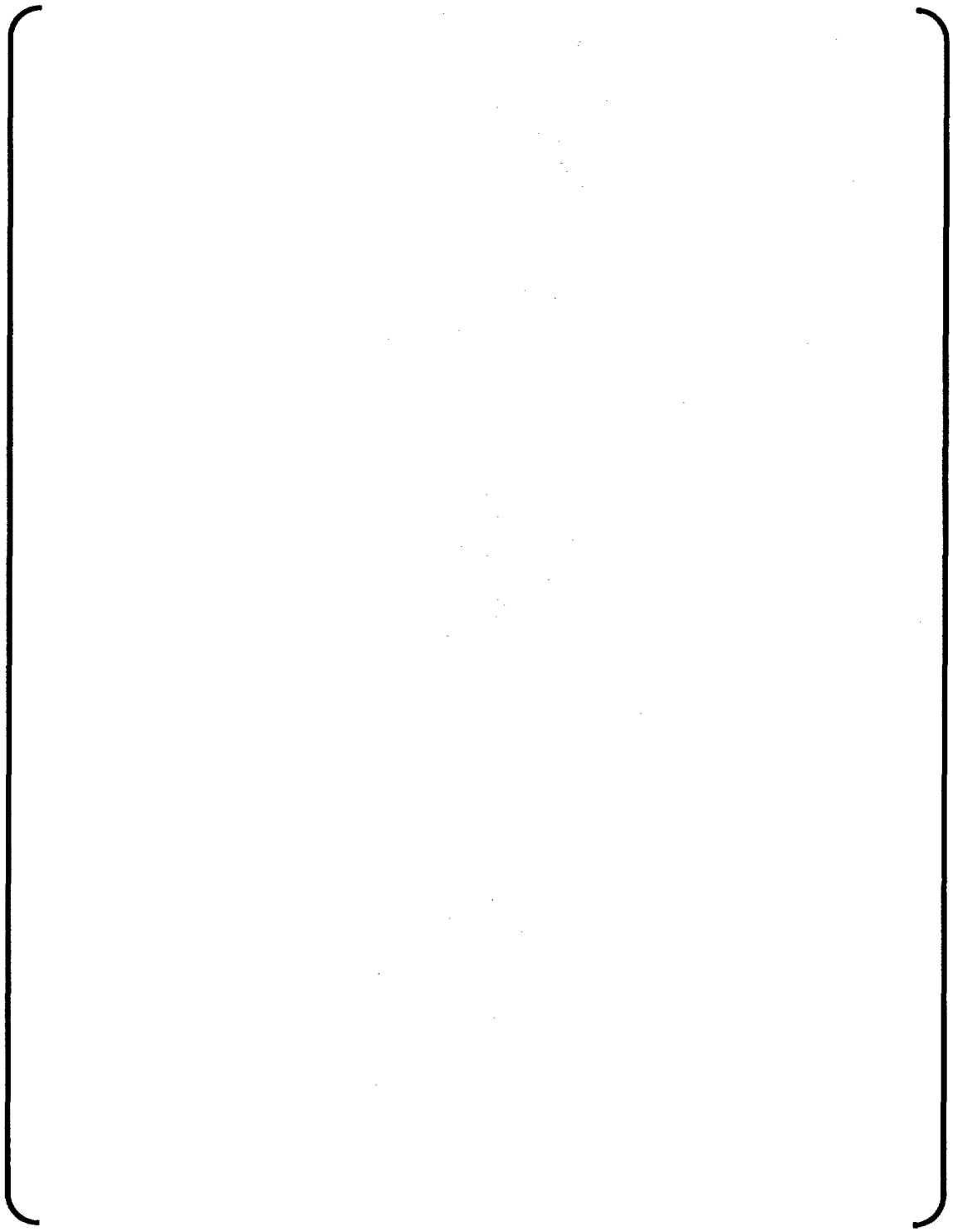

Figure B5-3
Stress Intensity Factor at Deepest Point of Circumferential Crack (Raju-Newman Solution): (a) Top of Weld, (b) One Row Above and (c) Two Rows Above

Confidential Commercial Information

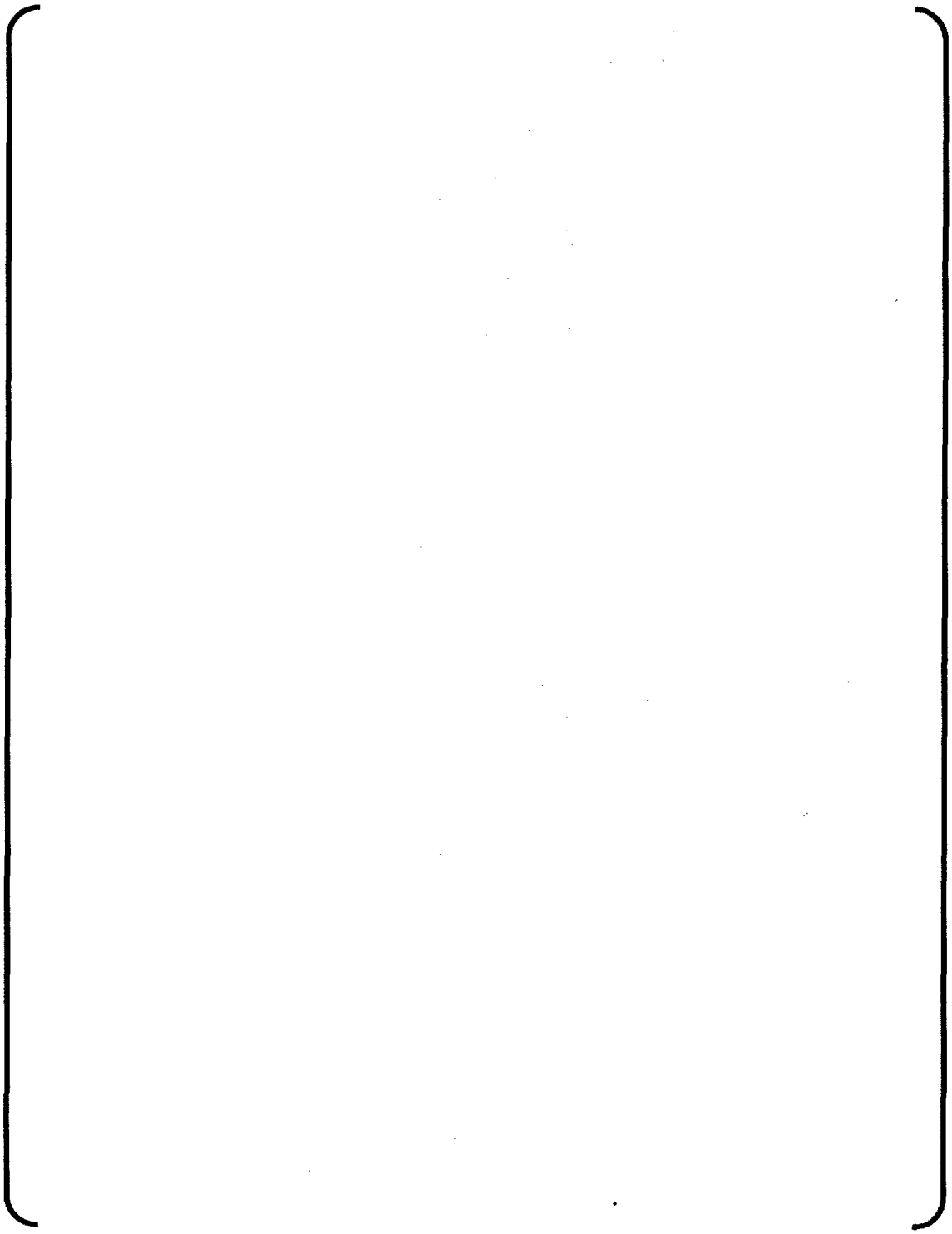

Figure B5-4
Stress Intensity Factor at Deepest Point of Circumferential Crack (ASME Section XI, A-3320): (a) Top of Weld, (b) One Row Above and (c) Two Rows Above

Appendix C

Gap Opening Displacement for BMV Leakage Detection

Analyses to confirm that there will be an operating condition gap between the CRDM nozzles and holes in the vessel heads, to ensure that there will be a leak path to the surface for bare metal visual inspections, were performed in October 2001 and are reported in DEI report R-3513-00-1, Revision 1, *Reactor Vessel Top Head Nozzle - Operating Fit Analysis – H.B. Robinson 2 Nuclear Power Plant* (53). The purpose of this appendix is to provide a brief overview of the analysis methodology and key results.

A finite element model was created of a sector of the vessel head as shown in Figures C-1 and C-2. The modeling of the nozzle shown in Figure C-3 reflects the zone of interference fit and the counterbore. Weld distortion was determined from analyses similar to that performed in Appendix A, and the resulting weld distortion was imposed on the gap model by applying constraint equations between the nozzle and weld. Figure C-4 shows the resultant weld distortion. Figure C-5 shows the flange rotation and equivalent stresses induced in the head as a result of the specified preload. Figure C-6 shows the equivalent stresses in the vessel head for operating conditions.

Figure C-7 shows the predicted gaps. The analysis shows that all nozzles have a predicted operating condition leak path to the top head surface for initial diametral interference fits of up to and including 0.00275" initial interference. Work also showed that for the small amount of possible interference in some nozzles, the actual metal-to-metal contact area is only about 5% of the nominal contact area. The remaining approximately 95% of the interference fit area will have small flow passages with an RMS height equal to the sum of the RMS surface roughness of the mating parts.

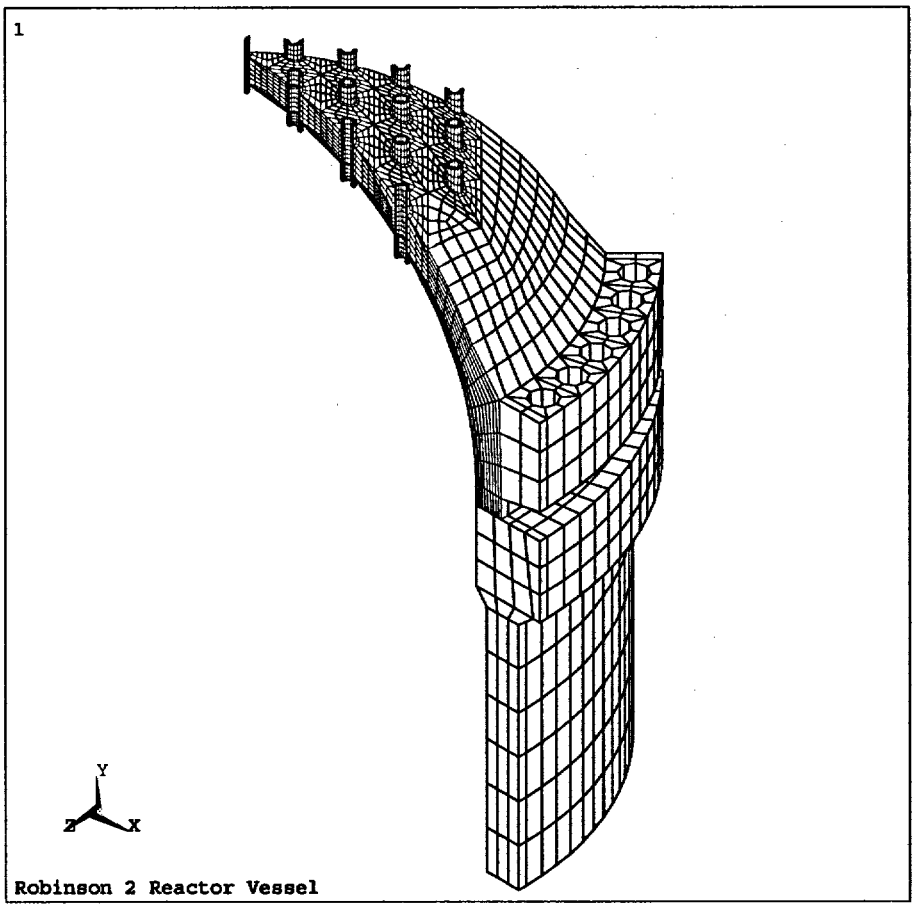

Figure C-1
Finite Element Model of Vessel Head

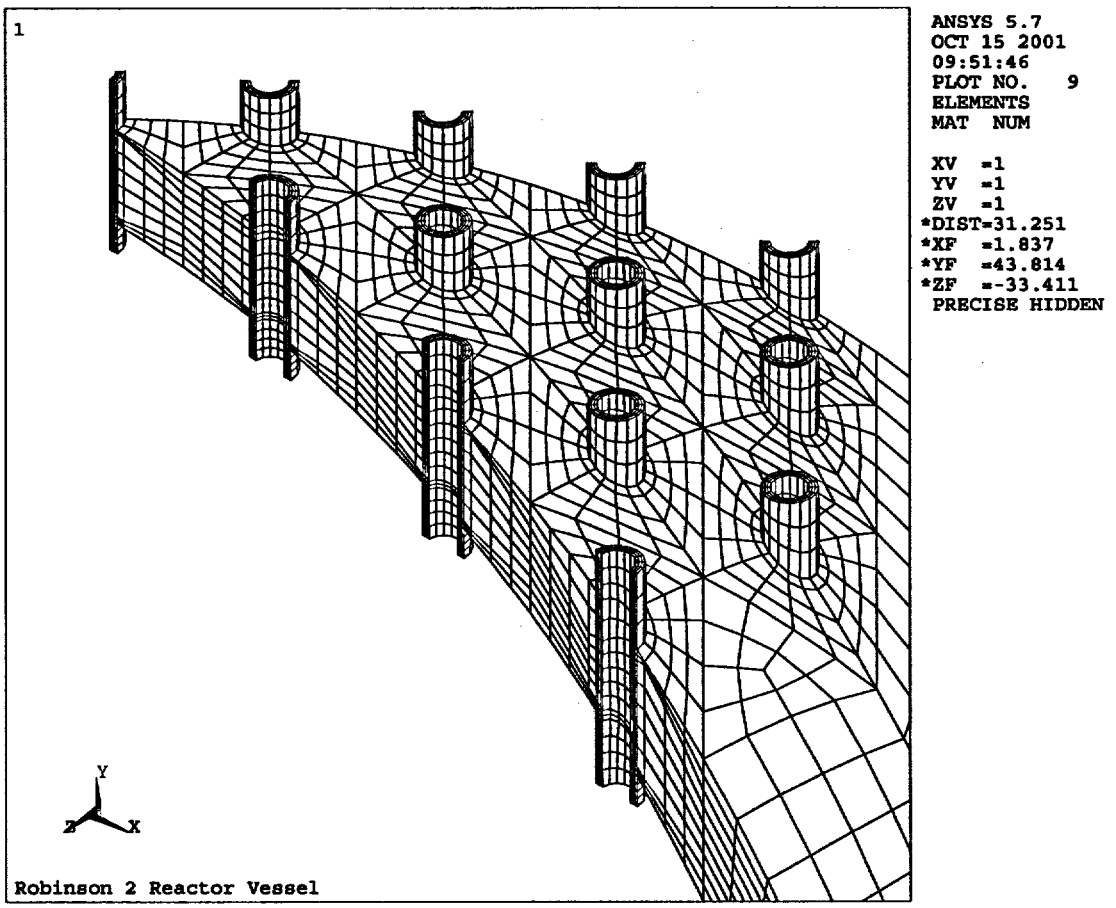

Figure C-2
Finite Element Model of Vessel Top Head CRDM Nozzle Region

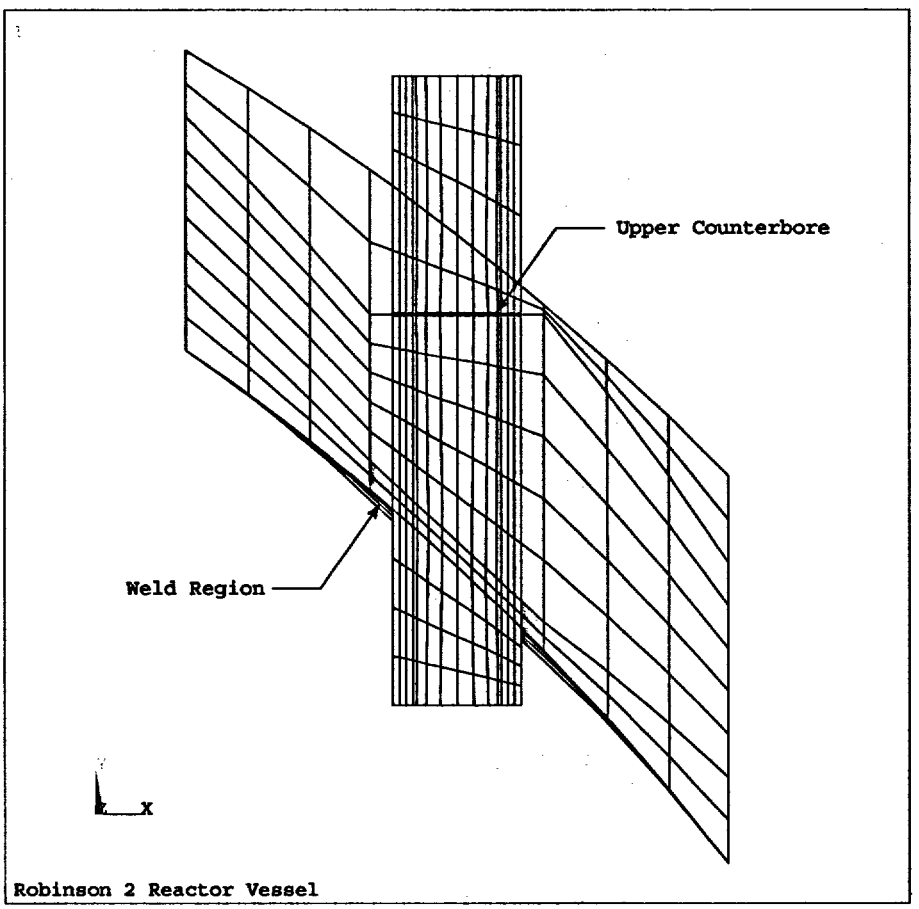

Figure C-3
Finite Element Model of CRDM Nozzle Module (Section View)

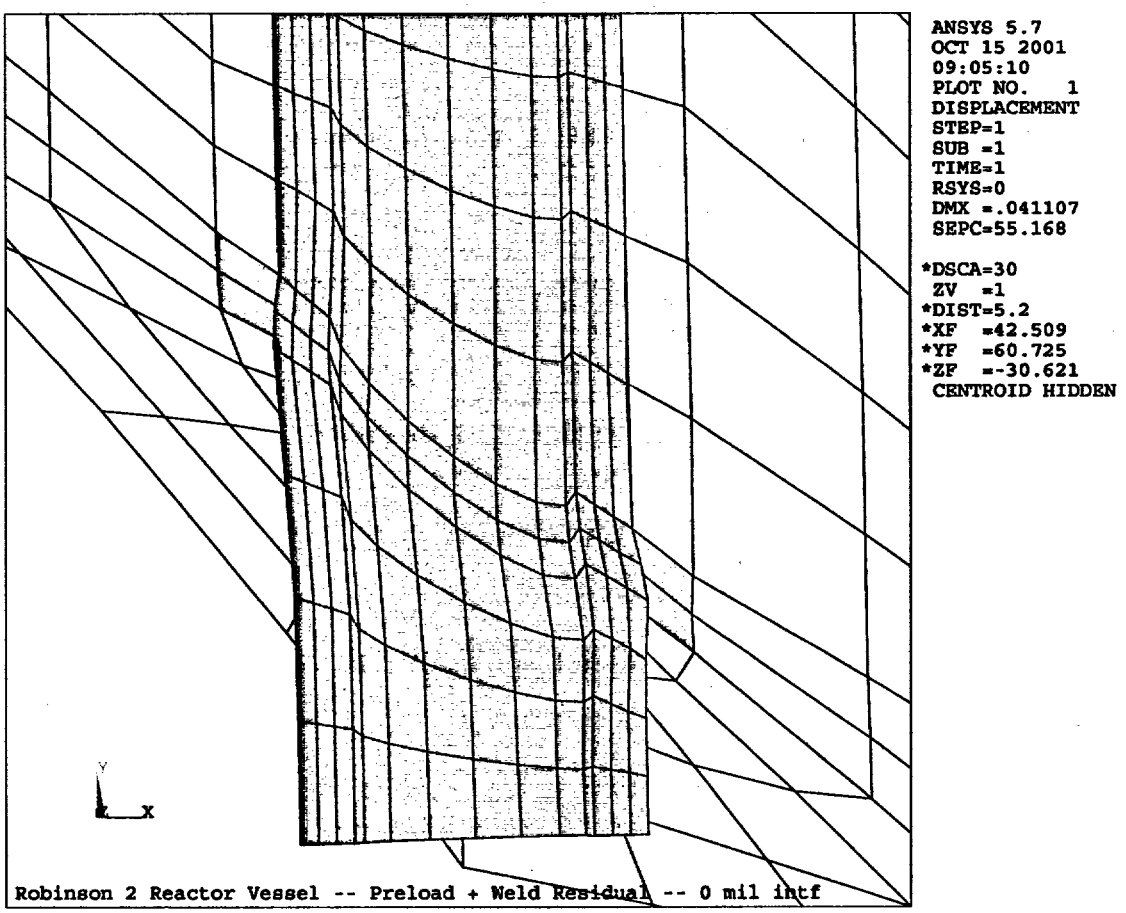

Figure C-4
Typical Deflections Imposed on Nozzle by J-Groove Weld

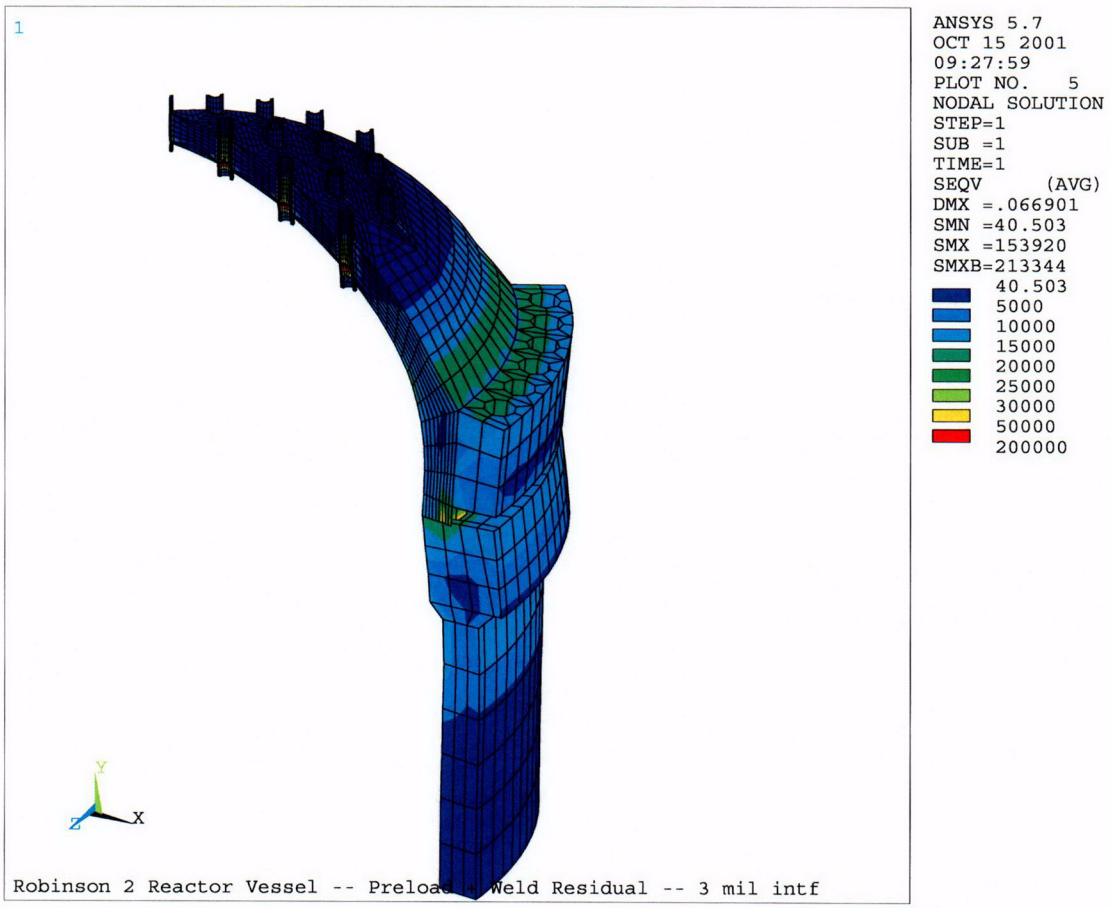

Figure C-5
Flange Rotation and Equivalent Stresses due to Flange Bolt Preload

C21

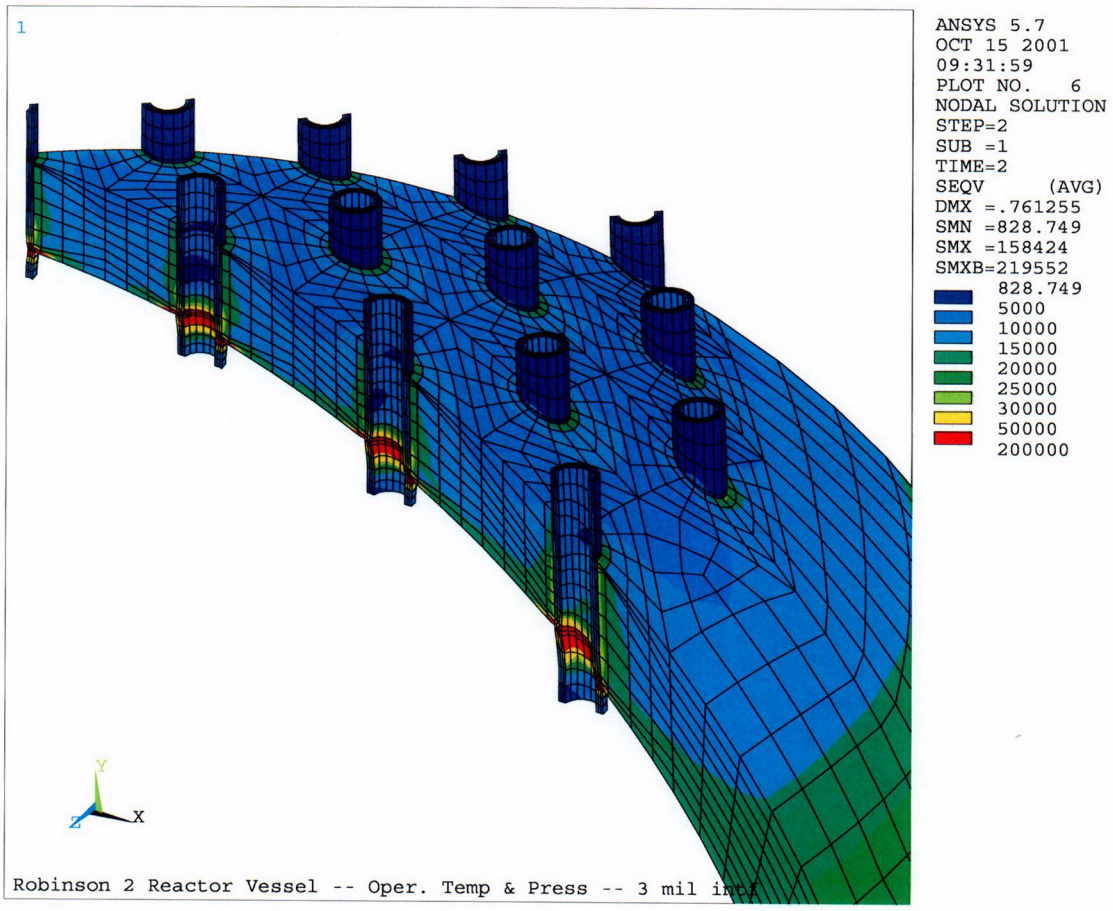

Figure C-6
Equivalent Stresses in Vessel Top Head Under Operating Conditions

C22

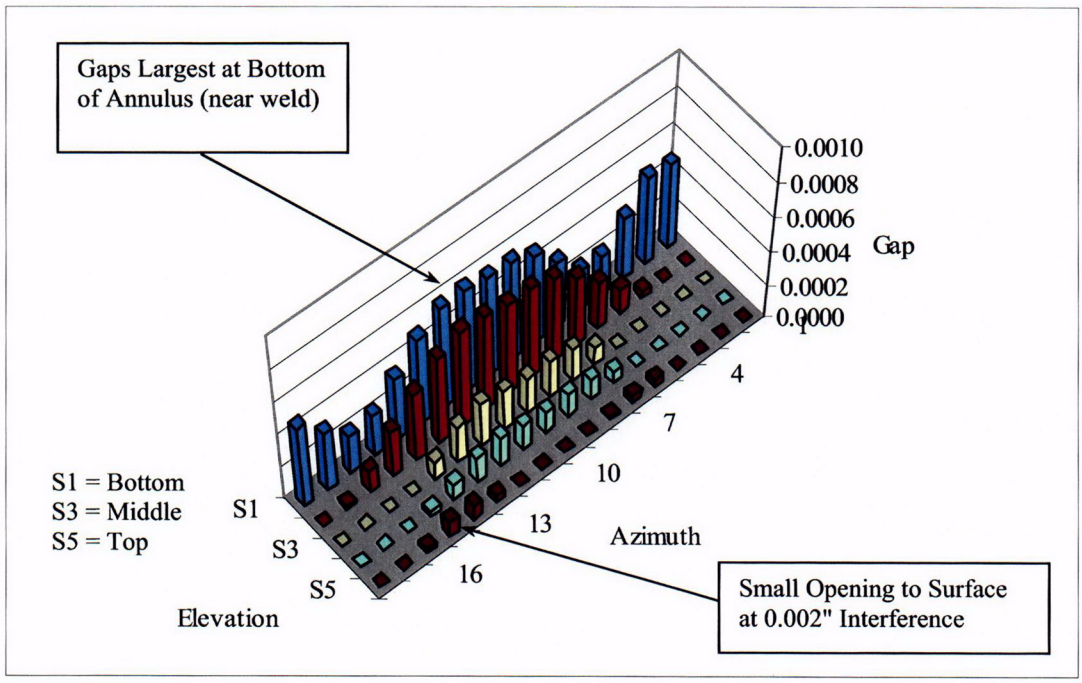

Figure C-7.a
Gap Opening Displacements for Nozzle #9
0.002" Initial Interference with Annulus Unpressurized

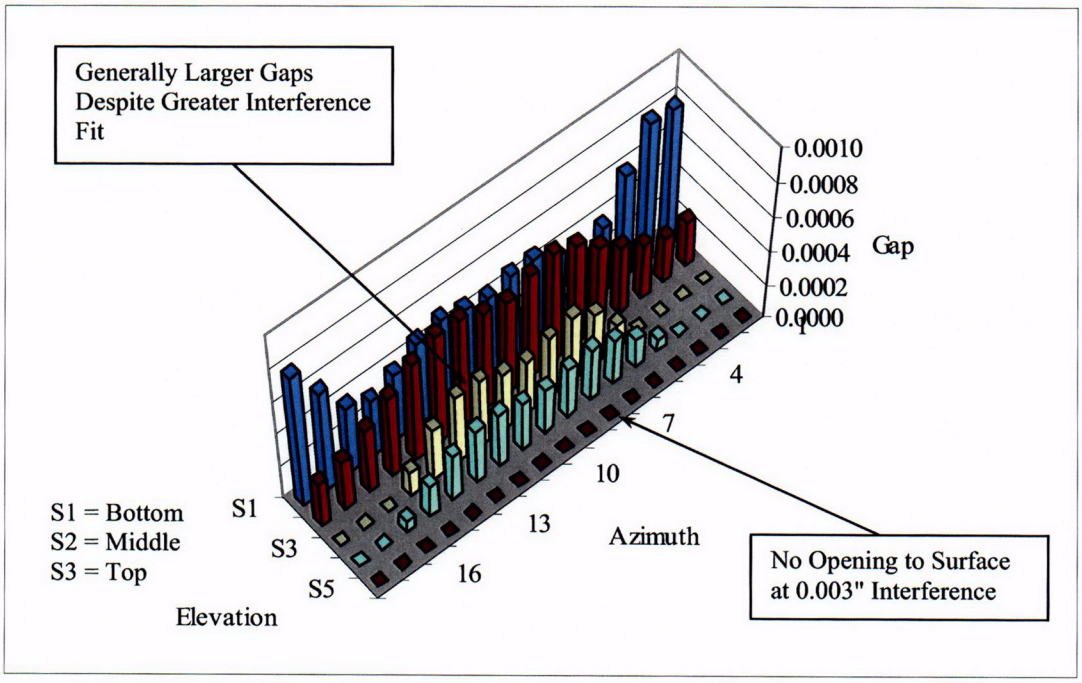

Figure C-7.b
Gap Opening Displacements for Nozzle #9
0.003" Initial Interference with Annulus Pressurized

C23

Appendix D

Allowable Wastage Volume

Attached calculation note C-3515-00-2, Revision 0, *H.B. Robinson RPV Head Allowable Wastage Volume Analysis*, provides results of finite element analyses to determine the amount of material that can be lost from the low-alloy steel vessel head by boric acid corrosion and still meet ASME Code primary membrane and primary membrane plus bending stress limits. The analysis methodology is the same as described in MRP-75, *PWR Reactor Pressure Vessel (RPV) Upper Head Penetrations Inspection Plan* (9). The results of this analysis are used in the probabilistic analyses in Section 8.

The contents of Appendix D are proprietary to DEI.

Confidential Commercial Information

[DEI Calculation C-3515-00-2, Revision 0, *H.B. Robinson RPV Head Allowable Wastage Volume Analysis*, is proprietary to Dominion Engineering, Inc., and has been removed from this non-proprietary version of Appendix D.]

Appendix E

Limiting Crack Sizes in Nozzles and Welds

Paragraph IWB-3640 (*Evaluation Procedures and Acceptance Criteria for Flaws in Austenitic and Ferritic Piping*) of Section XI of the ASME Boiler and Pressure Vessel Code (49) states that:

> *"A pipe containing flaws is acceptable for continued service for a specified evaluation time period if the criteria of IWB-3642, IWB-3643, or IWB-3644 are satisfied. The procedures shall be the responsibility of the Owner and shall be provided to the regulatory authority having jurisdiction at the plant site."*

Paragraph IWB-3644 (*Alternative Evaluation Procedure and Acceptance Criteria Based on Applied Stress*) of Section XI of the ASME Boiler and Pressure Vessel Code (49) states that:

> *"Piping containing flaws exceeding the allowable standards of IWB-3514.1 is acceptable for continued service until the end of the evaluation period if the alternative evaluation procedure demonstrates, at the end-of-evaluation period, safety factors, based on load equivalent to the following:*

Service Level	*Safety Factor*
A	*2.7*
B	*2.4*
C	*1.8*
D	*1.4*

The following are calculations for the maximum end-of-evaluation period flaws at three locations in the CRDM Nozzle shown in Figure E-1. These are 1) an axial through-wall flaw in the nozzle above the J-groove weld, 2) a through-wall partial arc circumferential flaw above the J-groove weld, and 3) a circumferential flaw at the fusion line between the nozzle and the J-groove weld. In each case, the analysis will show the limiting flaw size assuming design pressure and operating temperature conditions. Calculations have been performed for the central nozzle. The limiting flaw sizes will be greater for circumferential flaws and lack of fusion that follow the J-groove weld contour.

Per drawing E 232-284-5 (50), the nozzle OD is machined to 4.000" $^{+0.000"}/_{-0.001"}$, and the nozzle ID is 2-3/4" where the tolerance on fractional dimensions is ±1/64". The minimum OD is therefore, 3.999" and the maximum ID is 2.7656".

E.1 Axial Flaw in Nozzle Above J-Groove Weld

The limit pressure for a through-wall axial crack in a tube subjected to internal pressure loading is given by the EPRI, *Ductile Fracture Handbook* (NP-6301-D) (51) as follows:

$$P_{lim} = \sigma_f (t/R) / M \qquad \text{[Eq. E-1]}$$

where,

P_{lim} = limit pressure = 2.7 * design pressure = 2.7 (2,500 psi) = 6,750 psi

σ_f = tensile flow stress = 0.5 ($\sigma_y + \sigma_u$)

σ_y = yield strength at 599.7°F operating temperature = 29.9 ksi (@600°F)

σ_u = tensile strength at 599.7°F operating temperature = 80.0 ksi (@600°F)

D_o = minimum nozzle outside diameter = 3.999 in

D_i = maximum nozzle inside diameter = 2.7656 in

t = minimum nozzle wall thickness = $(D_o - D_i)/2$ = 0.6167 in

R = nozzle mean radius = $(D_o + D_i)/4$ = 1.6912 in

λ = $c/(Rt)^{0.5}$

c = half crack length

M = $[1 + 1.2987\,\lambda^2 - 2.6905\text{x}10^{-2}\,\lambda^4 + 5.3549\text{x}10^{-4}\,\lambda^6]^{0.5}$

Solving iteratively, an axial crack length of 5.3 inches results in a limit pressure of 6,750 psi. It should be noted that this calculation is conservative since the amount of crack opening displacement will be limited by the fit of the nozzle in the hole in the vessel head.

E.2 Circumferential Flaw in Nozzle Above J-Groove Weld

The limiting through-wall circumferential flaw is calculated using the method developed in MRP-44, Part 2 (52). The relatively tight fit of the nozzle in the vessel head will ensure that moment loads on the nozzle are low and that the limit load will be equal to the material flow stress acting on the remaining ligament. It is conservatively assumed for the calculation that 2.7 times the design pressure acts on the crack face as well as the nozzle bore diameter.

$$P_{lim} = \sigma_f \left[\frac{A_{wall}\left(1 - \frac{\theta}{360}\right)}{A_{bore} + A_{wall}\left(\frac{\theta}{360}\right)} \right] \qquad \text{[Eq. E-2]}$$

Solving for the crack angle θ that produces the limit pressure,

$$\theta = \frac{360\left[\sigma_f - P_{lim}\left(\frac{A_{bore}}{A_{wall}}\right)\right]}{P_{lim} + \sigma_f} \qquad \text{[Eq. E-3]}$$

where,

θ = circumferential crack length (degrees)

A_{bore} = nozzle bore area = $\pi D_i^2/4 = \pi(2.7656\text{ in})^2/4 = 6.007\text{ in}^2$

A_{wall} = nozzle wall area = $\pi(D_o^2 - D_i^2)/4$

= $\pi[(3.999\text{ in})^2 - (2.7656\text{ in})^2]/4 = 6.553\text{ in}^2$

A circumferential crack of 284° above the J-groove weld will support a pressure of 6,750 psi.

E.3 Lack of Fusion or Axial-Circumferential Weld Crack at J-Groove Weld Interface

The limiting area of lack of fusion between the nozzle and J-groove weld is calculated using the axial pressure load acting on the outside diameter of the nozzle and the allowable shear stress on the weld. The weld flow shear stress is taken as 50% of the nozzle base material flow stress.

$$0.5\sigma_f = \frac{P_{lim}\pi D_o^2/4}{\pi D_o H_{weld}\left[\frac{(360-\phi)}{360}\right]} \qquad \text{[Eq. E-4]}$$

$$\phi = 360 - 180\left(\frac{P_{lim}D_o}{\sigma_f H_{weld}}\right) \qquad \text{[Eq. E-5]}$$

where,

H_{weld} = minimum height of J-groove weld at nozzle wall

= 1.000 in

ϕ = circumferential lack of fusion length (degrees)

A circumferential area of lack of fusion between the weld and nozzle wall extending 271° around the nozzle will support a pressure of 6,750 psi.

Table E-1 is a summary of the limit flaw sizes presented above, plus the limit flaw sizes calculated using the design pressure with no safety factor. In summary, the nozzle will meet the ASME Code Section XI strength requirements with a through-wall axial flaw of about 5.3 inches

above the top of the J-groove weld, a through-wall circumferential flaw of about 284° above the top of the J-groove weld, or an area of lack of fusion between the nozzle and J-groove weld that extends about 271° around the nozzle. These significant size flaws are indicative of the structural margin inherent in the CRDM nozzle design.

Table E-1
Limit Flaw Sizes Based on the Design Pressure and Based on the Section XI Para. IWB-3644 Safety Factor for Continued Service with Actual Flaws

	2500 psi	6750 psi
Axial through-wall flaw in nozzle above J-weld	14.3 inches	5.3 inches
Circ. through-wall flaw above J-weld	330°	284°
Lack of fusion between nozzle and weld	327°	271°

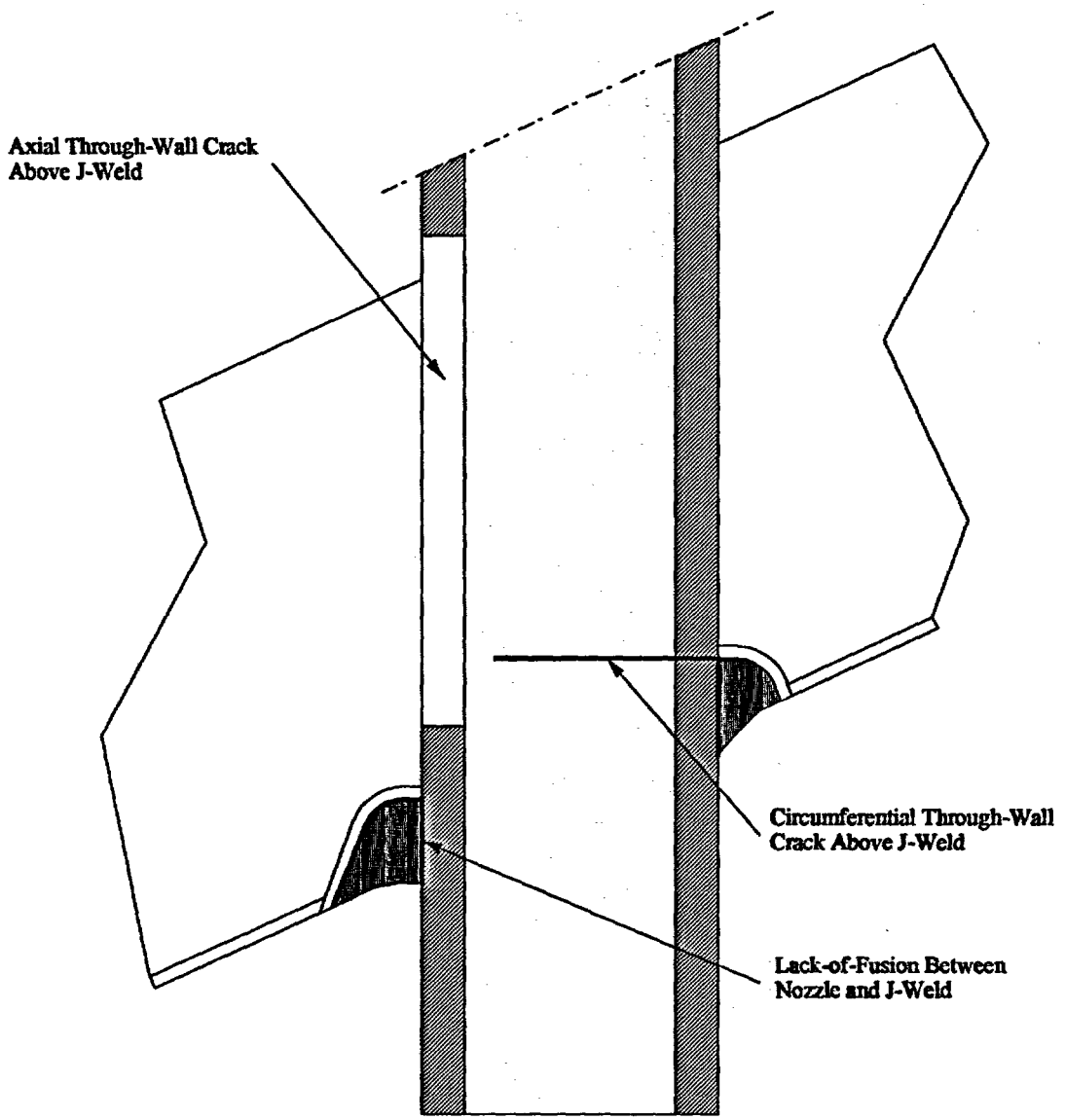

Figure E-1
Assumed Flaw Locations on Central CRDM Nozzle